SCIENTIFIC REPORTS

OPEN

Endogenous APOBEC3B Overexpression Constitutively Generates DNA Substitutions and Deletions in Myeloma Cells

Received: 31 October 2018
Accepted: 26 April 2019
Published online: 09 May 2019

Hiroyuki Yamazaki[1], Kotaro Shirakawa[1], Tadahiko Matsumoto[1], Shigeki Hirabayashi[1,2], Yasuhiro Murakawa[2,3], Masayuki Kobayashi[1], Anamaria Daniela Sarca[1], Yasuhiro Kazuma[1], Hiroyuki Matsui[1], Wataru Maruyama[1], Hirofumi Fukuda[1], Ryutaro Shirakawa[4], Keisuke Shindo[1], Masaki Ri[5], Shinsuke Iida[5] & Akifumi Takaori-Kondo[1]

Apolipoprotein B mRNA-editing enzyme catalytic polypeptide-like (APOBEC) DNA cytosine deaminases have emerged as potential genomic mutators in various cancers. Multiple myeloma accumulates APOBEC signature mutations as it progresses; however, the mechanisms underlying APOBEC signature acquisition and its consequences remain elusive. In this study, we examined the significance and clinical impact of APOBEC3B (A3B) activity in multiple myeloma. Among APOBECs, only highly expressed A3B was associated with poor prognosis in myeloma patients, independent of other known poor prognostic factors. Quantitative PCR revealed that CD138-positive primary myeloma cells and myeloma cell lines exhibited remarkably high A3B expression levels. Interestingly, lentiviral A3B knockdown prevented the generation of deletion and loss-of-function mutations in exogenous DNA, whereas in control cells, these mutations accumulated with time. A3B knockdown also decreased the basal levels of γ-H2AX foci, suggesting that A3B promotes constitutive DNA double-strand breaks in myeloma cells. Importantly, among control shRNA-transduced cells, we observed the generation of clones that harboured diverse mutations in exogenous genes and several endogenous genes frequently mutated in myeloma, including *TP53*. Taken together, the results suggest that A3B constitutively mutates the tumour genome beyond the protection of the DNA repair system, which may lead to clonal evolution and genomic instability in myeloma.

Multiple myeloma (MM) is a plasma cell malignancy that harbours a wide variety of genetic alterations, including base substitutions, translocations, copy number variations and aneuploidy[1,2]. MM develops from monoclonal gammopathy of undetermined significance (MGUS) by accumulating genomic DNA mutations during physiological B cell maturation[3]. According to the classic karyotypic classification system, MM/MGUS is divided into two subtypes: hyperdiploid, which is characterized by multiple trisomies of odd-numbered chromosomes and a lack of recurrent immunoglobulin gene translocations, and non-hyperdiploid, which is characterized by chromosome translocations t(4;14), t(14;16), t(14;20), t(6;14) and t(11;14)[4]. Among these karyotypic changes, ectopic expression of cyclin D is relatively often detected, either directly through its juxtaposition to an immunoglobulin enhancer and copy number amplification or indirectly through unidentified mechanisms[4]. Most of the translocations are caused by errors in immunoglobulin heavy chain (IgH) class switch recombination and V(D)J recombination[3], while the rest are caused by errors in somatic hypermutation during plasma cell development in germinal centers[5]. Thus, these translocations are referred to as primary translocations and are considered the primary steps of oncogenesis in normal plasma cells[6]. Based on its expression profiles, MM is divided into seven

[1]Department of Hematology and Oncology, Graduate School of Medicine, Kyoto University, Kyoto, 606-8507, Japan. [2]RIKEN-HMC Clinical Omics Unit, RIKEN Baton Zone Program, Kanagawa, 230-0045, Japan. [3]RIKEN Preventive Medicine and Diagnosis Innovation Program, Kanagawa, 230-0045, Japan. [4]Department of Molecular and Cellular Biology, Institute of Development, Aging and Cancer, Tohoku University, Sendai, 980-8575, Japan. [5]Department of Hematology and Oncology, Nagoya City University Graduate School of Medical Sciences, Nagoya, Japan. Correspondence and requests for materials should be addressed to A.T.-K. (email: atakaori@kuhp.kyoto-u.ac.jp)

signature groups similar to its cytogenetic classifications: CD-1 and CD-2 (CCND1/CCND3), HY (hyperdiploid), LB (low bone disease), MS (MMSET), MF (c-MAF/MAF-B) and PR (proliferation). These signature groups are correlated with clinical prognosis: MS, MF and PR are correlated with high risk and CD-1, CD-2, HY, and LB are correlated with low risk[7]. DNA hypomethylation, deletion of chromosome 13, MYC dysregulation, and driver mutations of *RAS* and *BRAF* are considered signs of malignant progression[8]. Particular translocations of the *MUM1*/*IRF4* (6p25), *MAFB* (20q11), *IRTA2* (1q21) and *MYC* (8q24) loci, which rarely involve immunoglobulin genes, are correlated with poor clinical outcomes[6]. Furthermore, during MM progression and relapse, additional genetic abnormalities such as dysregulation of the NF-κB pathway, loss of chromosome 17p and/or abnormalities of TP53 develop and contribute to achieving independence from the bone marrow microenvironment[4,8].

As with many other cancers, the presence of different subclones within MM tumours that are characterized by distinct genetic mutations independently contributes to MM progression[9]. High levels of intra-tumoural clonal heterogeneity and alterations in clonal dominance under therapeutic selective pressure have been described in patients with high-risk MM[10]. Hence, the molecular events underlying myeloma development and progression do no proceed in a linear fashion but rather through a Darwinian branching model[9–11]. Nevertheless, the causes of these events are largely unknown. Although activation-induced cytidine deaminase (AID) is considered to be responsible for early oncogenic processes, i.e., initiation of MM/MGUS, myeloma cells usually do not express AID[12] except when interacting with dendritic cells[13]. Strikingly, whole-genome sequencing has revealed that MM contains apolipoprotein B mRNA-editing enzyme catalytic polypeptide-like (APOBEC) signature mutations[11,14–16]. Accumulation of APOBEC signature mutations increases significantly during tumour recurrence and extramedullary extension[11] and is associated with poor prognosis[16,17]. Moreover, kataegis, which is defined by hypermutation in localized genomic regions and is supposedly generated by APOBECs[18], has been found at *MYC*/*IGK* or *IGL* translocation breakpoints[16], suggesting the co-occurrence of chromosomal translocations and APOBEC-associated mutations.

APOBEC3B (A3B) is an APOBEC cytidine deaminase that plays critical roles in immunity and is now highlighted as an intrinsic mutagen of genomic DNA that induces C-to-T and C-to-G substitutions, especially in breast cancer[19–22]. Among the seven APOBEC3 enzymes (APOBEC3A/B/C/DE/F/G/H; A3A–A3H), A3B is the only family member that is predominantly located in the nucleus throughout the cell cycle[23]. We previously reported that A3B induces C-to-T transitions in genomic DNA in human cell culture models[24]; therefore, we hypothesized that A3B might also induce DNA mutations in MM. In this study, we investigated the mutagenic activity of A3B in myeloma cells, and we here report how aberrantly expressed A3B induces DNA mutations and deletions and affects the survival of MM patients.

Results

A3B expression is aberrantly high in most malignant plasma cell samples from MM/MGUS patients and is associated with poor prognosis. First, we investigated the expression levels and genotypes of A3B in samples from MM/MGUS patients in our institutes. The patient characteristics are shown in Supplemental Table 1. MGUS patients accounted for 22.0% (n = 20), newly diagnosed multiple myeloma (NDMM) patients accounted for 45.1% (n = 41) and relapse/refractory MM (RRMM) patients accounted for 33% (n = 30) of a total of 91 patients. For 39 patients, we obtained the RNA of CD138+ myeloma cells from bone marrow samples to examine A3B expression. Because it was very difficult to obtain sufficient CD138-sorted plasma cells, PBMCs from healthy individuals were used as negative controls. Quantitative PCR analysis showed remarkably high expression levels of A3B in the majority of MM/MGUS patients (range, 0 to 1.214; median, 0.991; control vs MM/MGUS, $P = 0.00397$; control vs MM, $P = 0.001$; Fig. 1a, left panel). Regarding A3B genotypes, a deletion polymorphism that removes the entire A3B gene has been reported, and its frequency varies among major continental regions[25,26]. We examined the frequency of the A3B deletion allele in our patients and found that 44 were wild type (I/I, 48.4%; 95% CI, 37.7–59.1%), 40 were heterozygous (D/I, 44.0%; 95% CI, 33.6–54.8%), and 7 were homozygous for the deletion allele (D/D, 7.7%; 95% CI, 3.1–15.2%). There was no significant difference in allele frequency between MM/MGUS patients and Japanese healthy controls[26] (Supplemental Table 2), although the A3B deletion allele tended to be more prevalent in MGUS (15.0%; 95% CI, 3.2–37.9%) than in MM (5.6%; 95% CI, 1.6–13.8%) patients (Supplemental Table 2). A3B expression levels were significantly correlated with A3B genotype ($P = 0.0189$; Fig. 1a, middle panel) and showed a weak positive correlation with diagnosis (MGUS vs MM, $P = 0.0543$; Fig. 1a, left panel) but were not correlated with disease status (NDMM vs RRMM, $P = 0.642$; Fig. 1a, right panel).

Next, to investigate the clinical impact of each APOBEC, we analysed a microarray dataset of 414 NDMM patients from Arkansas University[7]. Among the APOBEC genes whose probes were available in the platform of the study, A3B expression reached very high levels (Supplemental Fig. 1a), although A3B is generally not expressed in normal tissues[27]. It has been recently described that patients with an absolute APOBEC signature contribution at diagnosis in the fourth quartile have worse progression-free survival and overall survival (OS) than patients in the first to third quartiles[17]. Thus, we divided the cohort into two groups: a high-APOBEC group including patients whose expression of each APOBEC as determined by microarray data was over the fourth quartile limit and a low-APOBEC group including patients with APOBEC expression under that limit. Importantly, only A3B was correlated with a significantly worse OS (A3B high group: 3-year OS, 66.2%; 95% confidence interval [CI], 52.9–76.5% vs A3B low group: 3-year OS, 81.8%; 95% CI, 75.6–86.5%; $P = 0.00133$; Supplemental Fig. 1b). Because A3B expression is correlated with known risk factors[16], we also assessed OS after risk group stratification based on genetic signatures[7] to exclude potential confounding biases. Consistent with a previous report[16], A3B expression differed significantly between the molecular subgroups (Supplemental Fig. 1c, $P = 1.17 \times 10^{-14}$). Univariate analysis showed that A3B expression levels still had a significant prognostic impact in the high-risk group (Supplemental Fig. 1d, right panel, $P = 0.00357$) as well as over long-term observation periods in the low-risk group (Supplemental Fig. 1d, left panel; $P = 0.143$, logrank test and $P = 0.00357$, 45-month

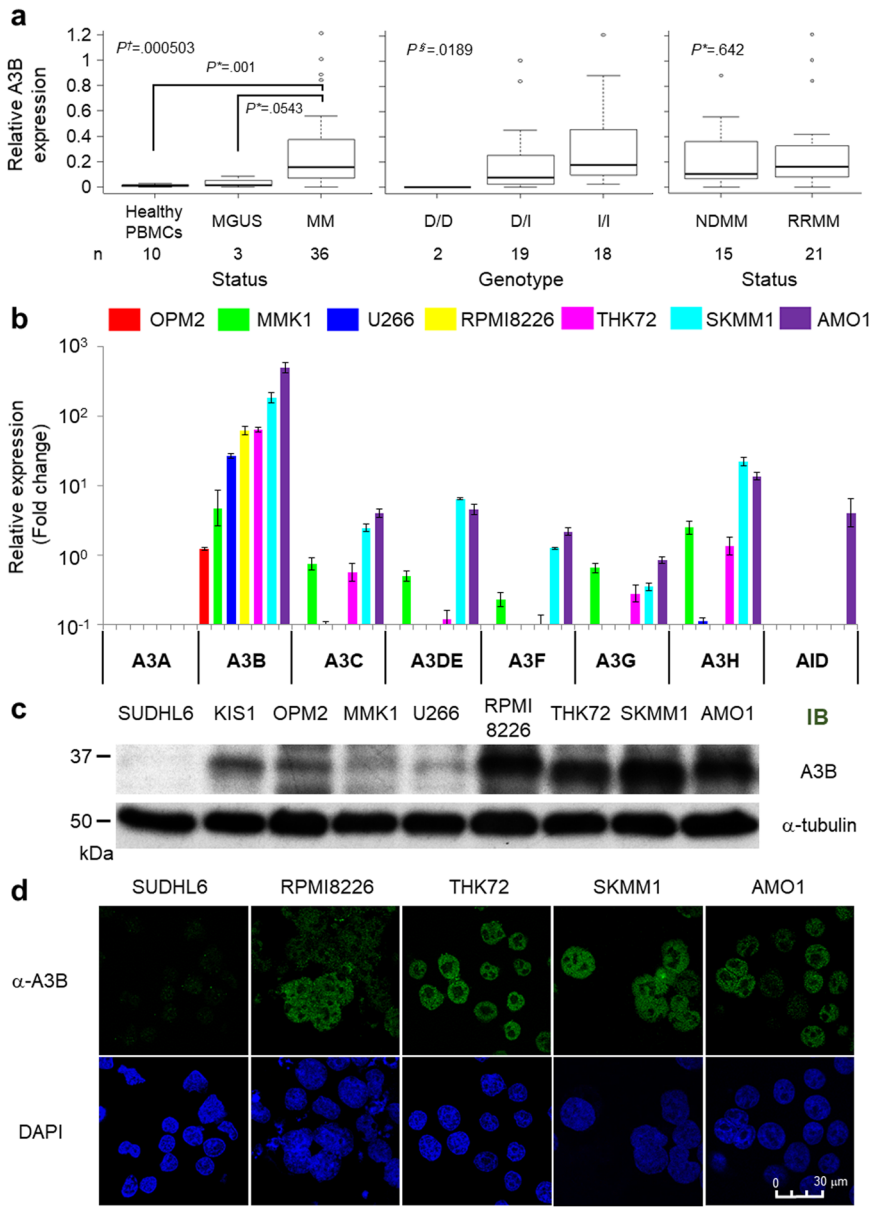

Figure 1. APOBEC family gene expression levels in MM/MGUS patients and myeloma cell lines. (**a**) Real-time PCR analysis of CD138-positive cells from MM/MGUS patient bone marrow. Statistical analysis of the correlation between A3B mRNA levels and diagnosis (healthy vs MGUS vs MM), genotype (D/D vs D/I vs I/I), or disease status (newly diagnosed MM [NDMM] vs relapse/refractory MM [RRMM]). The relative quantity of A3B mRNA was normalized by HPRT1 mRNA. *P* values were calculated using the Mann-Whitney U test (*), Kruskal-Wallis test (†) or Jonckheere-Terpstra test (§). (**b**) Real-time PCR of each of the APOBEC3 family genes (from A3A to A3H) and AID in seven myeloma cell lines (OPM2, MMK1, U266, RPMI8226, THK72, SKMM1 and AMO1). The target mRNA expression levels were normalized by HPRT1 mRNA levels. The target mRNA levels from PBMCs were used as a reference. (**c**) Immunoblot analysis of A3B in SUDHL6 cells (negative controls), KIS1 cells (positive controls) and the seven myeloma cell lines. α-Tubulin was evaluated as an internal control. (**d**) Fluorescence immunostaining using an anti-A3B antibody in SUDHL6, RPMI8226, THK72, SKMM1 and AMO1 cells. The images were obtained by confocal fluorescence microscopy (magnification, 630x).

landmark analysis). Univariate analysis also detected high A3C, high A3DE and low A3F as significant risk factors when the median was used as the threshold (Supplemental Table 3). However, only known risk and high A3B remained independent risk factors for OS after multivariate analysis following a Cox regression model (known high-risk group: hazard ratio [HR], 2.342; 95% CI, 1.503–3.649; $P = 0.0001693$ and high A3B: HR, 2.057; 95% CI, 1.294–3.270; $P = 0.0002305$; Supplemental Table 3).

A3B is highly upregulated and localized at the nucleoplasm in MM cell lines. We next investigated the expression profiles of AID and APOBEC3 family members in seven myeloma cell lines: OPM2, MMK1, U266,

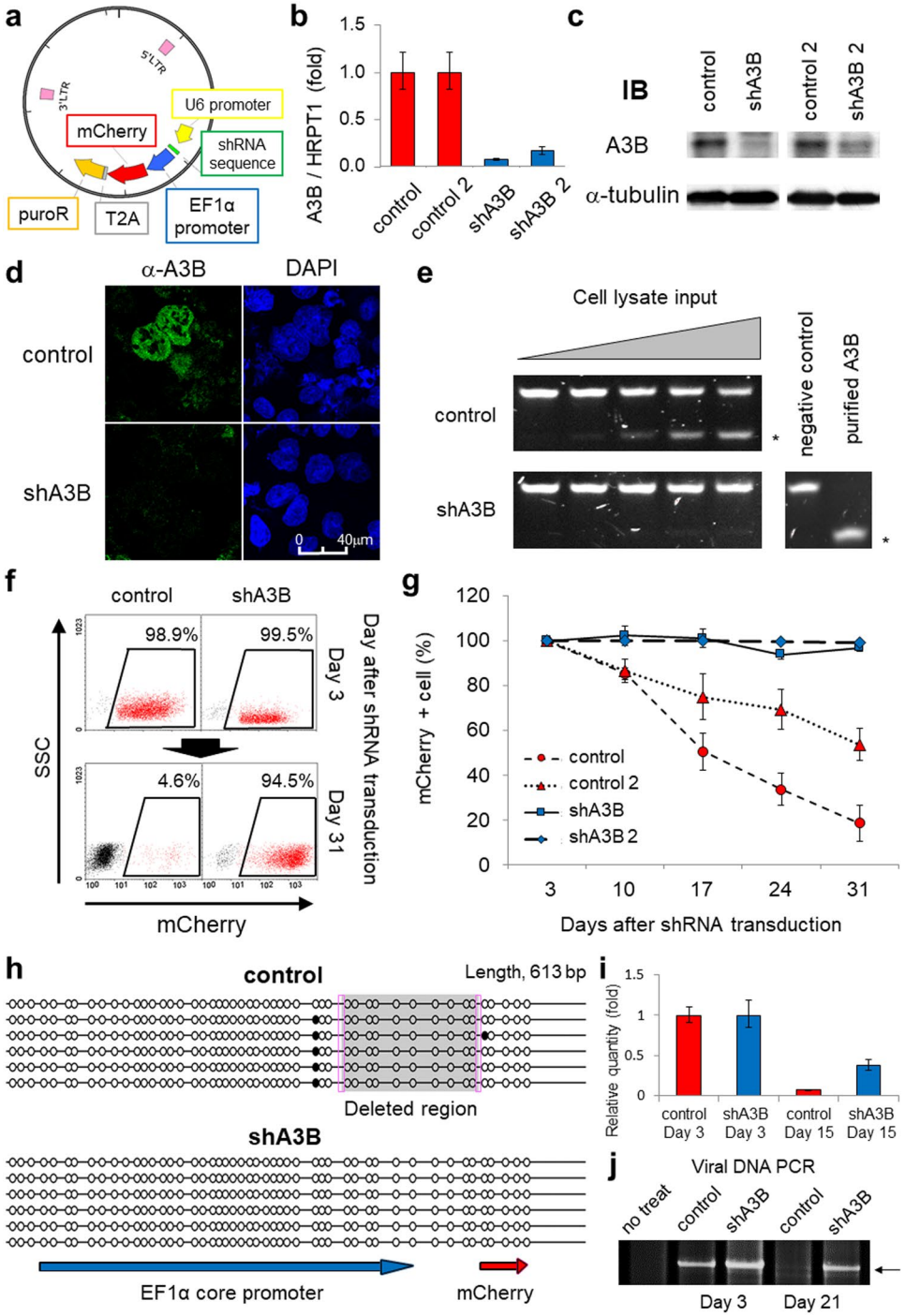

Figure 2. APOBEC3B mediates the loss of function of exogenous genes in myeloma cells. (**a**) Schema of the shRNA lentiviral vector construct. The produced lentivirus transduces shRNA together with mCherry and the puromycin resistance gene (puroR). (**b**,**c**) Real-time PCR (**b**) and immunoblotting (**c**) results of A3B levels in RPMI8226 cells, which were transduced with lentiviral shRNA against A3B (two constructs: shA3B and shA3B-2) or control shRNA (two constructs: control and control-2). HPRT1 or α-tubulin was evaluated as an internal control. (**d**) Immunofluorescence analysis using an anti-A3B antibody of RPMI8226 cells transduced with either shRNA against A3B or control lentivirus. The images were obtained by confocal fluorescence microscopy (magnification, 630x). (**e**) *In vitro* assay for cytidine deaminase activity in RPMI8226 cells transduced with either shRNA against A3B or control lentivirus. The asterisks indicates the cleaved DNA products. (**f**) Flow cytometry of RPMI8226 cells at 3 and 31 days after transduction with each mCherry-shRNA lentivirus. The numbers in boxes indicate the proportions of mCherry-positive cells among the live cells for each condition. (**g**) Time-dependent changes in the proportions of mCherry-positive cells among live cells transduced with each shRNA lentivirus as determined by flow cytometry. (**h**) Representative figure of the EF1α promoter methylation assay. The black circles represent methylated CpG. The shaded box indicates the deleted region. The sense strands of the EF1α promoter and a portion of the mCherry gene region are shown for reference. The pink boxes indicate

microhomology at the DNA double-strand breakpoint. (**i**) Real-time PCR of genomic mCherry. RPMI8226 genomic DNA expression at 3 and 15 days after transduction with each shRNA lentivirus was examined. *APOB* was evaluated as an internal control. The value at day 3 was used as a reference. (**j**) Conventional PCR of the full-length viral vector DNA. RPMI8226 genomic DNA expression at 3 and 21 days after transduction with each shRNA lentivirus was examined. The arrow indicates the amplicon size between the two LTR regions of the lentiviral vector (5200 bp).

THK72, RPMI8226, SKMM1 and AMO1. Consistent with the results from primary myeloma cells, these cell lines also expressed prominently high levels of A3B, as determined by quantitative PCR analysis (quantity relative to that in PBMCs: range, 1.22 to 489.4; median, 62.47; Fig. 1b). Cap analysis of gene expression (CAGE) in these seven myeloma cell lines showed that the activity of both A3B promoters was aberrantly upregulated compared to that in CD19+ cells from healthy individuals (Supplemental Fig. 2). We next determined protein expression levels using an anti-A3B antibody that we generated by immunizing rabbits with a C-terminal A3B peptide[28]. Because of the high homology of the C-termini, this anti-A3B antibody also detects artificially overexpressed A3A and A3G (Supplemental Fig. 3a,b). However, at endogenous expression levels, the antibody is more specific for A3B than for A3G (Supplemental Fig. 3c). We could also distinguish among these three proteins based on their sizes in immunoblot analyses (A3A, 25 kDa; A3B, 35 kDa; A3G, 40 kDa) and by their subcellular localization in immunofluorescence assays (A3A, cytoplasm and nucleus; A3B, nucleus; A3G, cytoplasm) (Supplemental Fig. 3a–c). We demonstrated that there was aberrant expression of A3B at the protein level in each MM cell line by immunoblotting (Fig. 1c) and confirmed A3B expression in the nuclei, but not in the nucleoli or in the cytoplasm, by using immunofluorescence assays (Fig. 1d); these findings were consistent with previous evidence[23].

Endogenous A3B overexpression contributes to loss of function of lentivirally introduced genomic DNA and to constitutive DNA double-strand breaks in myeloma cells. To assess the mutagenic activity of endogenous A3B in MM cells, we transduced RPMI8226 cells with lentiviral shRNA against A3B (shA3B) and with an EF1α-driven mCherry fluorescent marker (Fig. 2a). We confirmed A3B depletion at the mRNA and protein levels (Fig. 2b–d) and confirmed that there was little cytidine deaminase activity in shA3B-transduced cells (Fig. 2e). Notably, lentiviral shA3B transduction also efficiently decreased endogenous A3B expression in other MM cell lines, such as THK72, SKMM1 and AMO1, which are susceptible to lentivirus infection (Supplemental Fig. 3d,e). Interestingly, control shRNA-transduced cells lost mCherry fluorescence over a span of three weeks, whereas shA3B-transduced cells stably maintained it in the RPMI8226 cell line (Fig. 2f,g) as well as the THK72 and AMO1 cell lines (Supplemental Fig. 4a–d). To investigate this fluorescence loss, we determined the DNA methylation status of the EF1α promoter by bisulfite sequencing. DNA methylation was absent in both control shRNA- and shA3B-transduced cells, indicating that DNA methylation-mediated silencing did not cause the loss of fluorescence. Instead, we detected a large deletion accompanied by 6 bp microhomology (i.e., CGCCGT) at the junction point in the EF1α promoter in control shRNA-transduced cells (Fig. 2h). Using real-time PCR to quantify the copy number of the transduced mCherry genes, we detected a faster decrease in control shRNA-transduced cells than in shA3B-transduced cells (Fig. 2i). In addition, amplification of the full-length shRNA construct failed at day 21 in control shRNA-transduced cells (Fig. 2j). These data support the premise that the loss of fluorescence was caused by deletion mutations and/or ablation of the intact transduced gene.

Myeloma cells have been reported to exhibit constitutive DNA double-strand breaks (DSBs)[29]; therefore, we next investigated whether A3B knockdown changes the status of γ-H2AX, a DSB marker. shA3B transduction significantly reduced γ-H2AX protein levels, which was confirmed by fluorescence immunostaining in RPMI8226 and AMO1 cells (Fig. 3a,b) and immunoblot analysis in RPMI8226 cells (Fig. 3c,d). These results suggest that A3B contributes to constitutive DSBs leading to gene alterations in myeloma cells.

A3B constantly generates C>T|G>A transitions, which are then processed by the DNA repair system. We further tested the mutagenic activity of A3B by differential DNA denaturation PCR (3D-PCR), which efficiently amplifies DNA containing C>T|G>A transitions[30]. The mCherry sequences were amplified at lower denaturation temperatures in control shRNA-transduced than in shA3B-transduced RPMI8226 and AMO1 cells, both at Day 3 and at Day 21 after transduction (Fig. 4a). 3D-PCR of the puromycin resistance gene (puroR) also produced similar results (Fig. 4b). Using TA cloning and Sanger sequencing, we confirmed prominent G-to-A mutations in the mCherry gene (Fig. 4c and Supplemental Table 4) that are typical of the APOBEC signature (Fig. 4d). Intriguingly, we detected only G-to-A mutations, indicating that C-to-U deamination preferentially occurs in the antisense strand of the gene (Fig. 4c and Supplemental Table 4). Deep sequencing of the 3D-PCR products of the mCherry-T2A-puroR gene demonstrated that only G-to-A transitions accumulated throughout the gene and that the frequency of mutations increased towards the 3′ region of the gene (Fig. 4e and Supplemental Fig. 5a). Of note, Sanger sequencing of the 3D-PCR products showed that the occurrence of the C>T|G>A transition was similar between Day 3 and Day 21 (Fig. 4c). In contrast, deep sequencing of conventional PCR products of the mCherry gene failed to detect substitutions (Supplemental Fig. 5b). These findings demonstrate that mutations amplified by 3D-PCR occur in the presence (and occur less in the absence) of A3B in at least some fraction of cells or that DNA repair pathways might repair A3B-mediated DNA lesions. In fact, the 3D-PCR products of both control and shA3B-transduced cells contained large deletions that had at least 3-base microhomology at the junction points, suggesting that these mutations are at least in partly repaired by the microhomology-mediated end-joining (MMEJ) machinery[31] (Fig. 4f and Supplemental Table 4). The results of bisulfite sequencing of the EF1α promoter after conventional PCR also supported the involvement of MMEJ repair (Fig. 2h). Additionally, the combination of substitutions and deletions varied among the clones obtained from control cells, resulting in different amino acid sequences (Fig. 4f, Supplemental Tables 4 and 5). Abolition of the mCherry chromophore was predicted in clones

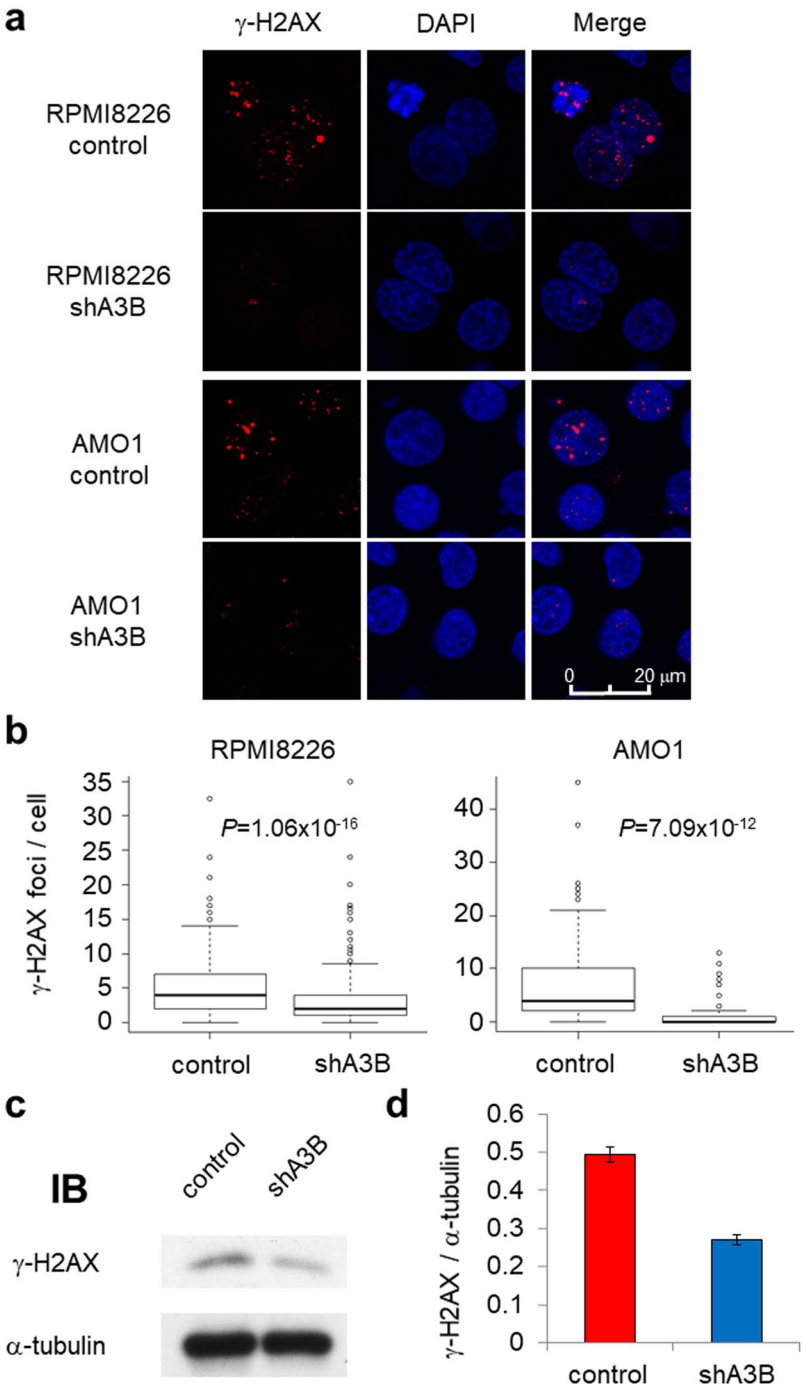

Figure 3. APOBEC3B promotes DNA double-strand breaks in myeloma cells. (**a**) Fluorescence immunostaining of γ-H2AX in RPMI8226 and AMO1 cells transduced with either control or A3B shRNA lentivirus. The images were obtained by confocal fluorescence microscopy (magnification, 630x). (**b**) Statistical analysis of the number of γ-H2AX foci per cell in RPMI8226 and AMO1 cells based on the images in (**a**). Approximately 200 cells were evaluated for each sample. All *P* values were calculated using Student's t test. (**c**) Immunoblot analysis of γ-H2AX in RPMI8226 cells transduced with either control or A3B shRNA lentivirus. (**d**) Bar graph of the γ-H2AX band intensities from (c) normalized by the α-tubulin band intensity.

that contained approximately hundreds of base deletions, suggesting that loss of mCherry fluorescence was at least partly caused by these deletion mutations (Supplemental Table 5).

We confirmed gene amplification at lower denaturation temperatures by 3D-PCR after shA3B transduction in two other A3B-expressing myeloma cell lines, including AMO1 (Fig. 4a, lower panel). Importantly, aurintricarboxylic acid and myricetin, which are known APOBEC3 deaminase inhibitors[32], also allowed for 3D-PCR amplification of the mCherry gene at lower denaturation temperatures in myeloma cells (Fig. 4g), suggesting that this cell-based model could be used for screening APOBEC3B inhibitors.

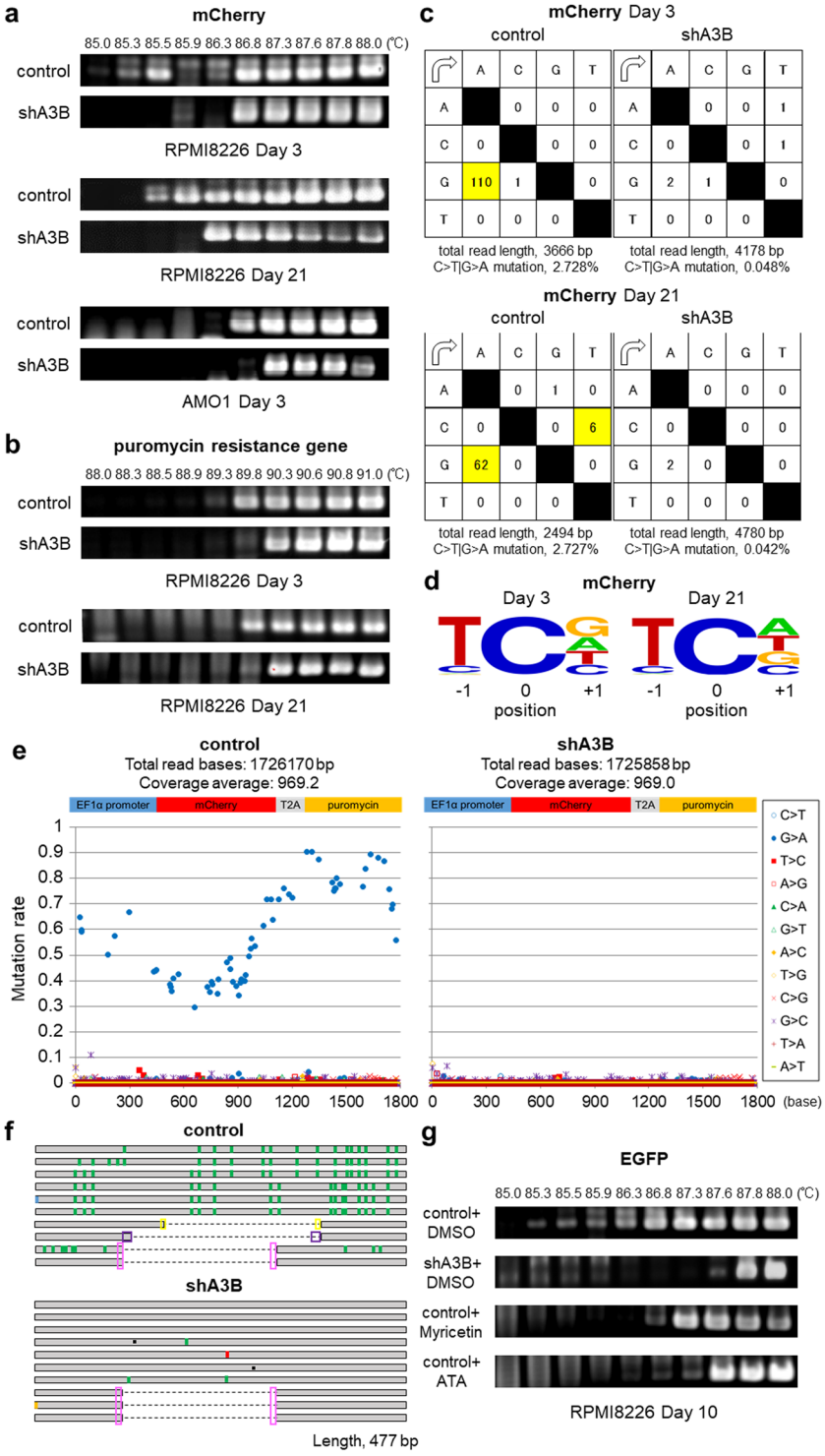

Figure 4. APOBEC3B induces C>T|G>A mutations in lentivirally introduced genomic DNA in myeloma cells. (**a**,**b**) 3D-PCR analysis of mCherry genes (**a**) and puromycin resistance genes (puroR) (**b**) derived from RPMI8226 genomic DNA at 3 or 21 days post transduction with each shRNA lentivirus. 3D-PCR analysis of mCherry genes derived from AMO1 genomic DNA at 3 days post transduction with each shRNA lentivirus is also indicated in (**a**). (**c**) Mutation matrices of hyperedited mCherry sequences derived from RPMI8226 genomic DNA at 3 (upper panel) and 21 (lower panel) days post transduction with each shRNA lentivirus. The sequence data were obtained by performing TA cloning and Sanger sequencing. The first column indicates the bases before mutation, and the first line indicates the bases after mutation. The highlighted boxes indicate significant C-to-T or G-to-A substitutions. The sense strand of the mCherry sequence was used as a reference. (**d**) Sequence logo created with WebLogo indicating the frequencies of nucleotides adjacent to C-to-T mutation sites. (**e**) Deep sequencing analysis of the 3D-PCR products of mCherry-T2A-puroR genes derived from RPMI8226 genomic DNA at 21 days post transduction with each shRNA lentivirus. The Y axis indicates the

proportion of each substitution in the total coverage, and the X axis indicates its location in the amplified gene from the EF1α promoter to the puroR gene. (**f**) Schema of Sanger sequencing results of each of the 10 clones of mCherry 3D-PCR products at 3 days post transduction with each shRNA lentivirus. G-to-A substitutions are indicated in green, C-to-T substitutions in red, G-to-C substitutions in light blue, and A-to-T substitutions in orange. The black squares indicate single-base deletions, whereas the dotted lines represent large deletions. The pink, purple or yellow boxes indicate microhomology at the DNA double-strand breakpoint. (**g**) 3D-PCR of *EGFP* derived from RPMI8226 genomic DNA at 10 days post transduction with control shRNA lentivirus under continuous incubation with the APOBEC3 inhibitors myricetin (5 μM) and aurintricarboxylic acid (ATA, 1 μM). We used lentiviral shRNA against APOBEC3B as a positive control.

Lastly, we examined the state of several endogenous genes that are known to be frequently mutated (e.g., *TP53* and *KRAS*) or in which breakpoints are observed in translocations frequently occurring in myeloma cells (e.g., in the *MYC* intergenic region)[8] (Fig. 5a). APOBEC signature mutations are known to be associated with DNA breakpoints[20]. Promoter regions of *BCL6* and *BCL7A* were also selected because cooperation between A3B and transcription factors has been reported[33]. Intriguingly, we detected significant 3D-PCR amplification of genes such as *TP53* and the *BCL6* and *BCL7A* promoters but little difference in *KRAS* (Fig. 5b). These data are consistent with previous reports showing that *TP53*-inactivating mutations are commonly found throughout the *TP53* gene and that *KRAS*-activating mutations are limited to hot spots (G12/G13/Q61/A146)[34]. We did not detect significant amplification in MYC intergenic regions, possibly because the MYC breakpoint is found in the megabase-wide intergenic region of *MYC*[35], while our primer sets for MYC 3D-PCR analysis only covered 700 and 679 base pairs (Fig. 5a). Sanger sequencing of the mutated *TP53* genes confirmed C>T|G>A transitions (Fig. 5c,d) and deletions (Fig. 5e), as summarized in Fig. 5f. We confirmed that these G>A|C>T transitions in *TP53* in the 3D-PCR product were reproducible in other cell lines, such as AMO1 and THK72 (Supplemental Fig. 6a–f). These results indicate that A3B mutates endogenous genes in genomic DNA as well as exogenous genes in transduced DNA, in our case the mCherry-T2A-puroR gene. These data suggest that most DNA substitutions induced by overexpressed A3B will be repaired by DNA repair pathways and that some clones will survive in the long term under selective pressure in myeloma cells.

Discussion

The present study demonstrates that endogenous A3B overexpression constitutively produces various combinations of C>T|G>A mutations and promotes DSB-related gene alterations in myeloma cells. Recent studies have demonstrated that there are clinical consequences of APOBEC activity in malignant tumours[36], especially in breast cancer[19,21]. Previous genome-wide analyses of MM/MGUS samples have also shown that mutation patterns associated with APOBEC activity correlate with disease progression and clinical outcomes[11,16,17], whereas those associated with AID activity contribute to disease initiation[37]. In ER-positive breast cancer, high A3B expression has been reported to correlate with treatment resistance, metastasis and poor prognosis[22,38], and there have been similar reports for lung cancer[39] and ovarian cancer[40]. Our analyses also show that aberrant A3B expression could have an impact on prognosis in MM patients, as A3B may contribute to disease progression and drug resistance. The present study is the first to specifically investigate the activity of endogenous A3B and to demonstrate its on-going mutagenic effects in myeloma cells. Importantly, A3B knockdown profoundly decreased the cytidine deaminase activity of whole-cell lysates from myeloma cells, suggesting that among APOBECs, A3B plays a major role in cytidine deamination-related mutagenesis in myeloma cells (Fig. 2e). On the other hand, breast cancer also shows APOBEC signature mutations in the absence of A3B, intimating the involvement of other APOBEC proteins, such as A3A[41] and A3H haplotype I[42]. A recent study showed that A3H haplotype I is associated with APOBEC signature mutations in lung and breast cancer[42]. We also found A3H to be relatively highly expressed in MM cell lines (Fig. 1b and Supplemental Fig. 2), suggesting the possible involvement of A3H-induced mutations in MM. Further studies are needed to confirm whether the A3H haplotype contributes to MM oncogenesis.

The precise mechanism of APOBEC-induced mutagenesis of genomic DNA is under intense investigation. Because APOBECs preferentially target single-stranded DNA (ssDNA), three situations have been proposed: first, that APOBECs target the lagging DNA strand under replication stress[43–45]; second, that they target ssDNA during the resection phase of homology-mediated repair after DSBs[20,36,43]; and third, that they target the non-transcribed strand during transcription[46–48]. Interestingly, in the present study, endogenous A3B deaminated cytosines mainly in the antisense strand (Fig. 4c,e and Supplementary Fig. 5a), suggesting that, instead, the transcribed strand might be the major A3B target. This discrepancy could have arisen due to differences in methodology; for example, 3D-PCR selectively amplifies minor clones of mutated DNA, whereas next-generation sequencing detects DNA mutations established through selection pressure or the DNA repair response.

Our data also suggested that lentivirally transduced genes lose their function due to deletions of hundreds of bases with microhomology at the junction points in A3B-overexpressing myeloma cells. It is plausible that multiplex attacks by A3B on ssDNA could cause DSBs, and subsequent MMEJ repair would produce a variety of clones harbouring deletions of various lengths. Whole-genome/exome sequencing with a coverage of tens to hundreds is usually able to detect only clones that account for more than a single-digit percentage of the total. Therefore, A3B-associated minor clones would be buried in sequencing errors and neglected. Since MMEJ repair of DSBs is undertaken at microhomology sequences near the breakpoint, clones with different DSB locations could be transformed into clones with the same deleted region. In fact, in our study, a number of clones with different combinations of mutations also had the same deleted region, as was revealed by TA cloning and Sanger sequencing (Figs 2h, 4f). However, most of the major mapping programs used for next generation sequencing, e.g., BWA and BWA-MEM[49,50], do not cover deletions of hundreds of bases such as the large deletions in mCherry

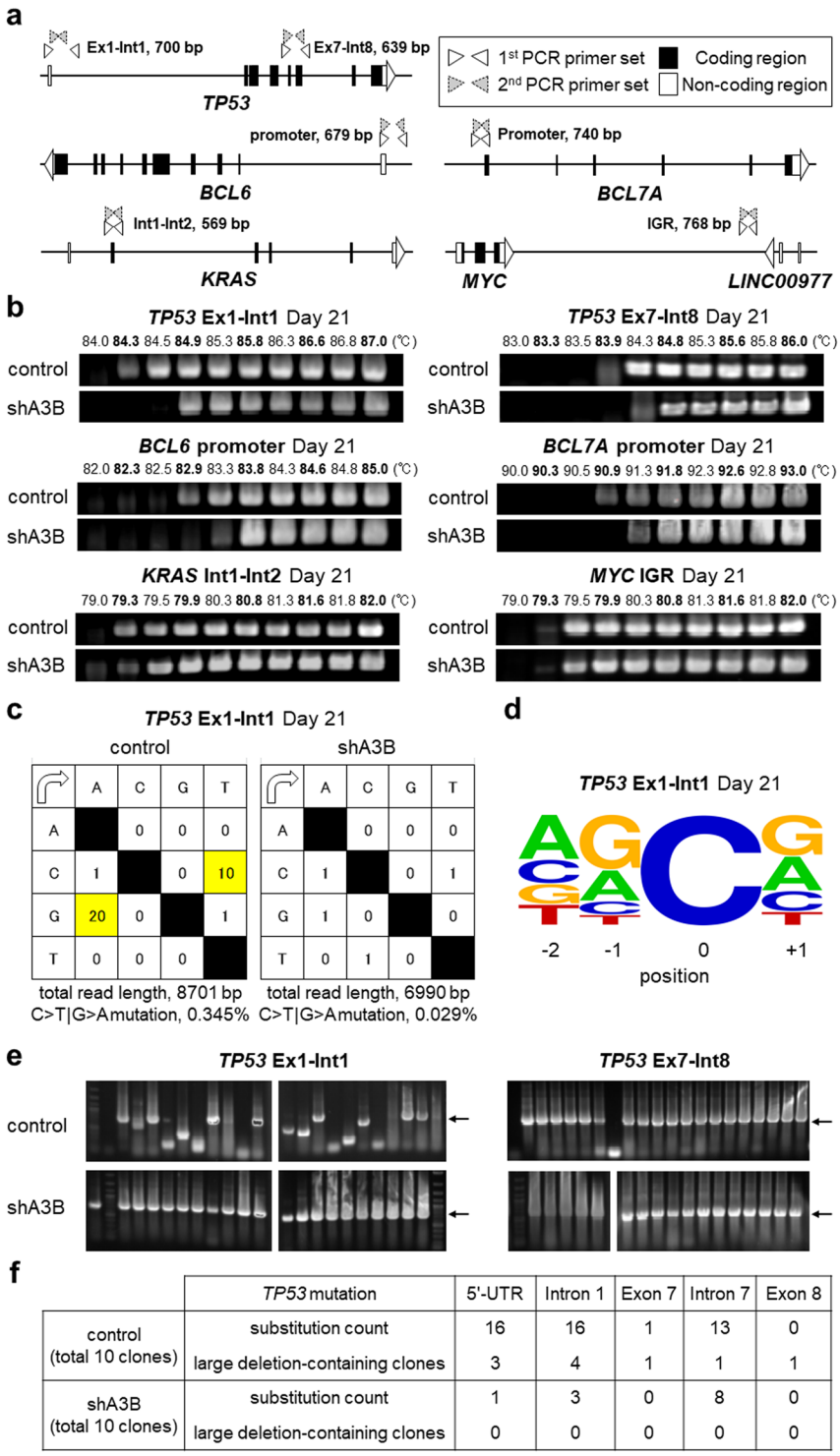

	TP53 mutation	5'-UTR	Intron 1	Exon 7	Intron 7	Exon 8
control (total 10 clones)	substitution count	16	16	1	13	0
	large deletion-containing clones	3	4	1	1	1
shA3B (total 10 clones)	substitution count	1	3	0	8	0
	large deletion-containing clones	0	0	0	0	0

Figure 5. APOBEC3B exerts its mutagenic activity on endogenous genes. (**a**) Primer settings for 3D-PCR of the endogenous genes of interest. The white boxes indicate 5′- or 3′-UTR sequences, and the black boxes indicate protein-coding sequences. The white and grey triangles represent the first and second PCR primer sets, respectively. (**b**) 3D-PCR of particular loci in genomic DNA obtained from RPMI8226 cells at 21 days post transduction with control or shA3B lentivirus. The loci include *TP53* from exon 1 (Ex1) to intron 1 (Int1) and from exon 7 (Ex7) to intron 8 (Int8), the *BCL6* promoter, the *BCL7A* promoter, *KRAS* from intron 1 (Int1) to intron 2 (Int2), and the *MYC* intergenic region (IGR). (**c**) Mutation matrices of hyperedited *TP53* sequences from Ex1 to Int1 obtained from RPMI8226 genomic DNA at 21 days post transduction with each shRNA lentivirus. The sequence data were obtained by performing TA cloning and Sanger sequencing. The first column indicates the bases before mutation, and the first line indicates the bases after mutation. The sense strand of *TP53* was used as a reference. C-to-T and G-to-A substitutions are highlighted. (**d**) Sequence logo created with WebLogo indicating the frequencies of nucleotides adjacent to C-to-T mutation sites in *TP53* Ex1-Int1. (**e**) Representative

colony PCR results for *TP53* from Ex1 to Int1 (left) and from Ex7 to Int8 (right) after TA cloning. Clones derived from control- or shA3B- transduced cells were selected from the PCR products obtained at the lowest denaturation temperatures in (**b**). The arrows indicate the intact sizes of the nested PCR products for *TP53* (700 bp and 639 bp). (**f**) Summary of Sanger sequencing for the 3D-PCR products of *TP53* Ex1-Int1 and Ex7-Int8.

(195 bp at minimum) detected in our study. Paired-end read analysis can detect structural variance, including large deletions of thousands of bases; nevertheless, sequenced reads that contain approximately hundreds of base deletions are unlikely to be mapped and will generally be discarded. Methods to obtain comprehensive snapshots of the production of minor clones *in vivo* still need to be validated.

Regarding mutation of endogenous genes, we observed enrichment of C-to-T substitutions and deletions in intronic regions and non-coding exons in the endogenous *TP53* gene, consistent with previous reports[8]. Chapman *et al*. demonstrated that the mutation frequency in coding regions was lower than that observed in UTR/promoter, intronic and intergenic regions in MM samples[8]. DNA repair responses, including transcription-coupled repair, might preferentially correct mutations in coding regions[51], or one or more unknown mechanisms might preferentially protect these regions from A3B attacks. Indeed, analysis of large whole-genome and exome datasets from bladder, cervical, breast, lung and head and neck cancers has indicated only a weak positive correlation between A3B expression and APOBEC-induced mutagenesis[36]. APOBEC-mediated mutations may develop as a result of the interplay between deaminase activity and the DNA damage response[52]. A limitation to using 3D-PCR for endogenous genes is the considerable PCR error rate. Suspene *et al*. stated that the 3D-PCR error rate is 0.02% owing to constant selection for AT DNA and PCR-mediated recombination[53]. In our study, the transition rate was 0.029% in the shA3B-derived genome, whereas in the control cells, the rate was elevenfold higher (0.345%, Fig. 5c). Accordingly, sequencing of the 3D-PCR products detected only background mutations in shA3B samples, but significantly more mutations were detected in control samples. Still, the mutational signature present in *TP53* appeared to be a complex cytosine mutation distribution rather than the typical A3B pattern (Fig. 5d). Previous studies on overexpressed A3B also showed similar results[24,54], and the authors discussed the possibility that the intrinsic preference of A3B was skewed by downstream repair pathways or other mutation-generating processes[54]. Our data showing that mutational signatures were different between exogenous and endogenous genes despite the use of the same DNA inputs may support their hypothesis. Regarding the substitution rate, C>T|G>A transitions were much more frequent in the exogenous genes (2.728% in mCherry-T2A-puroR, Fig. 4c) than in the endogenous genes (0.345% in *TP53*, Fig. 5c) of control samples. One of the reasons behind these different rates might be that lentivirally transduced genes are processed by the DNA repair system differently than endogenous genomic genes. Further studies are needed to clarify this issue.

In conclusion, aberrantly highly expressed endogenous A3B can contribute to genomic instability and therefore to linear and branched clonal evolution in the context of long-term disease progression. Although the clinical impact of A3B-related oncogenesis in myeloma remains to be further evaluated, inhibiting A3B activity could protect against disease deterioration and could be a new therapeutic option.

Materials and Methods

Clinical samples. All investigations have been conducted in accordance with ethical standards and have been approved by the Institutional Review Boards of Kyoto University and Nagoya City University, respectively. Written informed consent for the banking and subsequent research using their specimens, including genomic studies, was obtained from each patient. Bone marrow mononuclear cells were first obtained after centrifugation of bone marrow aspirates using the Lympholyte®-H (CEDARLANE) density gradient separation medium, and then myeloma cells were further isolated using the MACS CD138 positive cell isolation kit (Miltenyi Biotec). To assess the A3B polymorphism, the intact (I) and deletion (D) alleles were genotyped as previously described[55].

Cell lines and cell culture. Six human myeloma cell lines, OPM2, U266, RPMI8226, THK72[56], SKMM1 and AMO1, and two B-cell lymphoma cell lines, SUDHL6 and KIS1[28], were maintained in RPMI1640 (Nacalai) containing 10% FBS and 1% PSG (Invitrogen). The MMK1 myeloma cell line was established in our laboratory by culturing primary myeloma cells from the pleural effusion of a refractory myeloma male patient.

Quantitative RT-PCR. Total RNA was extracted from clinical samples and cell lines using the High Pure RNA isolation kit (Roche). Complementary DNA was synthesized using the PrimeScriptR II 1st strand cDNA Synthesis Kit (Takara) by random primer and oligo dT primer mixture. Real-time PCR was performed using the Thunderbird SYBR qPCR Mix (ToYoBo). Target gene expression levels were normalized by endogenous expression levels of HPRT1. To assess the copy number of introduced mCherry genes in lentivirally transduced cells, genomic DNA was extracted using the QuickGene DNA whole blood kit S (KURABO) and was evaluated and normalized by the endogenous APOB allele. All primers for real-time PCR are listed in Supplemental Table 6.

CAGE analysis. Promoter-level gene expression analysis was performed using CAGE[57]. Total RNA from each cell line was isolated using the RNeasy Mini Kit (Qiagen) and assessed with the Agilent RNA6000 Nano Kit (Agilent Technologies). 5 μg of total RNA (RIN > 7, A260/280 and 260/230 ratios > 1.7) was used for CAGE library preparation. CAGE libraries were made based on no-amplification non-tagging CAGE libraries for Illumina next-generation sequencers (nAnT-iCAGE) as previously described[57]. After Illumina sequencing, we used the MOIRAI pipeline[58] to remove ribosomal RNA (rRNA) sequences and sequences with base 'N', and to align the reads. In the pipeline, rRNAdust (http://fantom.gsc.riken.jp/5/suppl/rRNAdust/) was used to remove rRNA with rRNA sequences (U13369.1) and the parameters of −e 2 and −t 8. Mapping to the hg19 reference genome was done using bwa -aln (version 0.5.9)[49] with the parameters of −n 0.02, −o 1, −e −1, −i 5, −d 10, −l

32, −k 2, −m 2000000, −t 8, −M 3, −O 11, −E 4, −R 30, −q 0. Using samtools version 0.1.8[59], the resultant SAM files were converted to BAM files and low-quality nucleotides (MAPQ < 10) were filtered out. 5′ ends of reads were counted on FANTOM5-defined CAGE peaks[60] based on the annotation file retrieved on April 25th, 2017 from the link below. Tags per million (TPM) normalized expression values were used. (http://fantom.gsc.riken.jp/5/datafiles/latest/extra/CAGE_peaks/hg19.cage_peak_phase1and2combined_ann.txt.gz.)

Immunoblot analysis. Whole cell lysates were subjected to immunoblot analysis using a purified rabbit anti-A3B polyclonal antibody, a mouse anti-phospho-histone H2A.X (Ser139) antibody (Millipore, clone JBW301) or a mouse anti-α-tubulin monoclonal antibody (AA13, Funakoshi). The anti-A3B antibody was generated from a rabbit immunized with the C-terminal peptide EEHSQALSGRLRAILQNQGN by Sigma Aldrich as previously described[28].

Knockdown experiments. We constructed pSicoR-mCherry/EGFP lentiviral vectors[61] expressing short-hairpin RNA (shRNA) against A3B by inserting synthetic double-stranded oligonucleotides (TRCN0000140546[19], sense oligo, 5′-TGCAAAGCAATGTGCTCCTGATCTCGAGATCAGGAGCACATTGCTTTGCTTTTTTC-3′, and antisense oligo, 5′-TCGAGAAAAAAGCAAAGCAATGTGCTCCTGATCTCGAGATCAGGAGCACATTGCTTTGCA-3′; TRCN0000139463, sense oligo, 5′-TCCTGATGGATCCAGACACATTCTCGAGAATGTGTCTGGATCCATCAGGTTTTTTC-3′, and antisense oligo, 5′-TCGAGAAAAAACCTGATGGATCCAGACACATTCTCGAGAATGTGTCTGGATCCATCAGGA-3′) into the cloning site. For non-target shRNA, we used two constructs that were cloned as scrambled sequences (control[62], sense oligo, 5′-TGTCAAGTCTCACTTGCGTCTTCAAGAGAGACGCAAGTGAGACTTGACTTTTTTC-3′, antisense oligo, 5′-TCGAGAAAAAGTCAAGTCTCACTTGCGTCTCTCTTGAAGACGCAAGTGAGACTTGACA-3′; control-2[63], sense oligo, 5′-TATCTCGCTTGGGCGAGAGTAAGCTCGAGCTTACTCTCGCCCAAGCGAGATTTTTTTC-3′, antisense oligo, 5′-TCGAGAAAAAAATCTCGCTTGGGCGAGAGTAAGCTCGAGCTTACTCTCGCCCAAGCGAGATA). The lentivirus was produced by co-transfection of Trans-Lentiviral packaging plasmid mix (GE Dharmacon) and pSicoR-mCherry/EGFP into Lenti-X cells. Physical particle titers were measured using the RETRO-TEK HIV-1 p24 Antigen ELISA kit (ZeptoMetrix) and matched titers of each lentiviral vector (control vs shA3B) were used.

A3B catalytic domain biochemistry. The DNA deamination assay was performed as previously described[64]. Cell lysates were mixed with a 6-FAM labeled 43-long oligonucleotide containing a TTCC deamination site for 30 min at 37 °C before adding uracil DNA glycosylase and NaOH to create and break an abasic site. The samples were separated on 15% acrylamide-urea gels and analyzed with the Gel Doc EZ system.

3D-PCR and Deep sequencing. For DNA editing assays, genomic DNA was extracted as described above from myeloma cells at 3 and 21 days after transduction by pSicoR-mCherry shRNA lentivirus. We performed 3D-PCR[30] by amplifying genes using the KOD FX Neo (ToYoBo) DNA polymerase as described before[24]. All primer sets and conditions are listed in Supplemental Table 6. For Sanger sequencing, amplicons derived at the lowest temperature were incubated with A-attachment Mix (ToYoBo) and were subsequently cloned into the T-vector pMD20 (TaKaRa). Each extracted plasmid from DH5α cells (ToYoBo) transformed with the cloned vector was sequenced using the 3130xl Genetic Analyzer (Applied Biosystems). For deep sequencing analysis, amplicons (5 ng) derived at the lowest temperature were sheared and sequenced on an Illumina NextSeq instrument to obtain 75 nucleotides paired end reads. After Illumina sequencing, low-quality nucleotides (MAPQ < 10) were discarded and then Illumina sequencing adapters and primers sequences were removed from the reads. Finally, the reads were aligned using the BWA-MEM algorithm with default settings (version 0.7.12)[50].

Immunofluorescence assays. Myeloma cells were air-dried and fixed in 4% paraformaldehyde in phosphate-buffered saline (PBS) for 20 minutes on glass slides using Shandon cytospin 2 (THERMO FISHER SCIENTIFIC). Fixed cells were permeabilized, reduced and denatured for 30 minutes in PBS buffer containing 0.5% SDS, 5% β-mercaptoethanol and 10% FBS. Then, cells were washed three times with PBS containing 4% FBS and 0.1% Triton X-100 (PFT buffer)[65], and incubated with a purified rabbit anti-A3B antibody for 1 hour. Subsequently, cells were incubated with a goat anti-rabbit IgG (H + L)-Alexa Fluor® 488 preadsorbed antibody (Abcam, ab150081) for 30 min in the dark. γ-H2AX foci analysis was performed as previously described[29] using a mouse anti-phospho-histone H2A.X (Ser139) antibody (Millipore, clone JBW301) as primary antibody and a goat anti-mouse IgG (H + L)-Alexa Flour® 594 preadsorbed antibody (Abcam, ab150120) as secondary antibody. All antibodies were diluted with 3% BSA and 0.5% Tween in PBS. Around two hundred cells were observed and scored with a confocal laser scanning microscope (TCS-SP8, Leica) or a fluorescence microscope (BZ-9000, KEYENCE).

Bisulfite sequencing analysis. To examine CpG methylation levels in the EF1α promoter region transduced by the pSicoR lentiviral vector, 500 ng of extracted genomic DNA was converted using the MethylEasy Xceed kit (Human Genetic Signatures). First-round PCR was performed by Quick Taq HS DyeMix (ToYoBo) using 25 ng of converted DNA in a 10 μl reaction mixture, then 0.5 μl of the first-round PCR product was used as template for nested PCR in a 25 μl reaction mixture. All primer sets and conditions are listed in Supplemental Table 6.

Datasets. To examine the association between A3B expression and clinical outcomes, we used the Arkansas dataset (GSE4581)[7], which consists of MAS5 normalized gene expression profiles generated using the Affymetrix U133Plus2.0 microarray platform and clinical information from the Multiple Myeloma Genomics Portal (MMGP) (http://portals.broadinstitute.org/mmgp/home).

Statistical analysis. Descriptive statistics included absolute and relative frequencies for categorical data and median, mean, and range for numerical measurements. Mann-Whitney U test, Kruskal-Wallis test or Jonckheere-Terpstra trend test were used to evaluate the differences in continuous variables between two groups or more than three groups. Probabilities of OS were calculated based on Kaplan-Meier product limit estimates, and the OS outcomes of the two groups divided according to APOBECs expression levels were compared using the Logrank test. *P* values less than 0.05 were considered statistically significant. Multivariate analysis was performed using a Cox proportional hazard model for OS. Covariates with a P value < 0.2 factor in the univariate analysis were entered into the model. All statistical analyses were performed with EZR (Saitama Medical Center, Jichi Medical University), which is a graphical user interface for R (The R Foundation for Statistical Computing, version 3.0.2)[66].

References

1. Avet-Loiseau, H. *et al.* Genetic abnormalities and survival in multiple myeloma: the experience of the Intergroupe Francophone du Myelome. *Blood* **109**, 3489–3495, https://doi.org/10.1182/blood-2006-08-040410 (2007).
2. Avet-Loiseau, H. *et al.* Prognostic significance of copy-number alterations in multiple myeloma. *Journal of clinical oncology: official journal of the American Society of Clinical Oncology* **27**, 4585–4590, https://doi.org/10.1200/JCO.2008.20.6136 (2009).
3. Walker, B. A. *et al.* Characterization of IGH locus breakpoints in multiple myeloma indicates a subset of translocations appear to occur in pregerminal center B cells. *Blood* **121**, 3413–3419, https://doi.org/10.1182/blood-2012-12-471888 (2013).
4. Chesi, M. & Bergsagel, P. L. Molecular pathogenesis of multiple myeloma: basic and clinical updates. *Int J Hematol* **97**, 313–323, https://doi.org/10.1007/s12185-013-1291-2 (2013).
5. Bergsagel, P. L. & Kuehl, W. M. Chromosome translocations in multiple myeloma. *Oncogene* **20**, 5611–5622, https://doi.org/10.1038/sj.onc.1204641 (2001).
6. Kuehl, W. M. & Bergsagel, P. L. Multiple myeloma: evolving genetic events and host interactions. *Nature reviews. Cancer* **2**, 175–187, https://doi.org/10.1038/nrc746 (2002).
7. Zhan, F. *et al.* The molecular classification of multiple myeloma. *Blood* **108**, 2020–2028, https://doi.org/10.1182/blood-2005-11-013458 (2006).
8. Chapman, M. A. *et al.* Initial genome sequencing and analysis of multiple myeloma. *Nature* **471**, 467–472, https://doi.org/10.1038/nature09837 (2011).
9. Walker, B. A. *et al.* Intraclonal heterogeneity and distinct molecular mechanisms characterize the development of t(4;14) and t(11;14) myeloma. *Blood* **120**, 1077–1086, https://doi.org/10.1182/blood-2012-03-412981 (2012).
10. Magrangeas, F. *et al.* Minor clone provides a reservoir for relapse in multiple myeloma. *Leukemia* **27**, 473–481, https://doi.org/10.1038/leu.2012.226 (2013).
11. Bolli, N. *et al.* Heterogeneity of genomic evolution and mutational profiles in multiple myeloma. *Nat Commun* **5**, 2997, https://doi.org/10.1038/ncomms3997 (2014).
12. Pasqualucci, L. *et al.* Expression of the AID protein in normal and neoplastic B cells. *Blood* **104**, 3318–3325, https://doi.org/10.1182/blood-2004-04-1558 (2004).
13. Koduru, S. *et al.* Dendritic cell-mediated activation-induced cytidine deaminase (AID)-dependent induction of genomic instability in human myeloma. *Blood* **119**, 2302–2309, https://doi.org/10.1182/blood-2011-08-376236 (2012).
14. Alexandrov, L. B. *et al.* Signatures of mutational processes in human cancer. *Nature* **500**, 415–421, https://doi.org/10.1038/nature12477 (2013).
15. Cifola, I. *et al.* Whole-exome sequencing of primary plasma cell leukemia discloses heterogeneous mutational patterns. *Oncotarget* **6**, 17543–17558, https://doi.org/10.18632/oncotarget.4028 (2015).
16. Walker, B. A. *et al.* APOBEC family mutational signatures are associated with poor prognosis translocations in multiple myeloma. *Nat Commun* **6**, 6997, https://doi.org/10.1038/ncomms7997 (2015).
17. Maura, F. *et al.* Biological and prognostic impact of APOBEC-induced mutations in the spectrum of plasma cell dyscrasias and multiple myeloma cell lines. *Leukemia* **32**, 1044–1048, https://doi.org/10.1038/leu.2017.345 (2018).
18. Lada, A. G. *et al.* AID/APOBEC cytosine deaminase induces genome-wide kataegis. *Biology direct* **7**, 47; discussion 47, https://doi.org/10.1186/1745-6150-7-47 (2012).
19. Burns, M. B. *et al.* APOBEC3B is an enzymatic source of mutation in breast cancer. *Nature* **494**, 366–370, https://doi.org/10.1038/nature11881 (2013).
20. Taylor, B. J. *et al.* DNA deaminases induce break-associated mutation showers with implication of APOBEC3B and 3A in breast cancer kataegis. *Elife* **2**, e00534, https://doi.org/10.7554/eLife.00534 (2013).
21. Cescon, D. W., Haibe-Kains, B. & Mak, T. W. APOBEC3B expression in breast cancer reflects cellular proliferation, while a deletion polymorphism is associated with immune activation. *Proc Natl Acad Sci USA* **112**, 2841–2846, https://doi.org/10.1073/pnas.1424869112 (2015).
22. Sieuwerts, A. M. *et al.* Elevated APOBEC3B correlates with poor outcomes for estrogen-receptor-positive breast cancers. *Hormones & cancer* **5**, 405–413, https://doi.org/10.1007/s12672-014-0196-8 (2014).
23. Lackey, L., Law, E. K., Brown, W. L. & Harris, R. S. Subcellular localization of the APOBEC3 proteins during mitosis and implications for genomic DNA deamination. *Cell cycle (Georgetown, Tex.)* **12**, 762–772, https://doi.org/10.4161/cc.23713 (2013).
24. Shinohara, M. *et al.* APOBEC3B can impair genomic stability by inducing base substitutions in genomic DNA in human cells. *Scientific reports* **2**, 806, https://doi.org/10.1038/srep00806 (2012).
25. Kidd, J. M., Newman, T. L., Tuzun, E., Kaul, R. & Eichler, E. E. Population stratification of a common APOBEC gene deletion polymorphism. *PLoS genetics* **3**, e63, https://doi.org/10.1371/journal.pgen.0030063 (2007).
26. Imahashi, M. *et al.* Lack of association between intact/deletion polymorphisms of the APOBEC3B gene and HIV-1 risk. *PLoS One* **9**, e92861, https://doi.org/10.1371/journal.pone.0092861 (2014).
27. Refsland, E. W. *et al.* Quantitative profiling of the full APOBEC3 mRNA repertoire in lymphocytes and tissues: implications for HIV-1 restriction. *Nucleic acids research* **38**, 4274–4284, https://doi.org/10.1093/nar/gkq174 (2010).
28. Maruyama, W. *et al.* Classical NF-kappaB pathway is responsible for APOBEC3B expression in cancer cells. *Biochem Biophys Res Commun* **478**, 1466–1471, https://doi.org/10.1016/j.bbrc.2016.08.148 (2016).
29. Herrero, A. B., San Miguel, J. & Gutierrez, N. C. Deregulation of DNA double-strand break repair in multiple myeloma: implications for genome stability. *PLoS One* **10**, e0121581, https://doi.org/10.1371/journal.pone.0121581 (2015).
30. Suspene, R., Henry, M., Guillot, S., Wain-Hobson, S. & Vartanian, J. P. Recovery of APOBEC3-edited human immunodeficiency virus G->A hypermutants by differential DNA denaturation PCR. *The Journal of general virology* **86**, 125–129, https://doi.org/10.1099/vir.0.80426-0 (2005).
31. Sinha, S., Villarreal, D., Shim, E. Y. & Lee, S. E. Risky business: Microhomology-mediated end joining. *Mutation research* **788**, 17–24, https://doi.org/10.1016/j.mrfmmm.2015.12.005 (2016).
32. Li, M. *et al.* First-in-class small molecule inhibitors of the single-strand DNA cytosine deaminase APOBEC3G. *ACS Chem Biol* **7**, 506–517, https://doi.org/10.1021/cb200440y (2012).

33. Periyasamy, M. *et al*. APOBEC3B-Mediated Cytidine Deamination Is Required for Estrogen Receptor Action in Breast Cancer. *Cell Rep* **13**, 108–121, https://doi.org/10.1016/j.celrep.2015.08.066 (2015).
34. Walker, B. A. *et al*. Identification of novel mutational drivers reveals oncogene dependencies in multiple myeloma. *Blood* **132**, 587–597, https://doi.org/10.1182/blood-2018-03-840132 (2018).
35. Walker, B. A. *et al*. Translocations at 8q24 juxtapose MYC with genes that harbor superenhancers resulting in overexpression and poor prognosis in myeloma patients. *Blood cancer journal* **4**, e191, https://doi.org/10.1038/bcj.2014.13 (2014).
36. Roberts, S. A. *et al*. An APOBEC cytidine deaminase mutagenesis pattern is widespread in human cancers. *Nature genetics* **45**, 970–976, https://doi.org/10.1038/ng.2702 (2013).
37. Bolli, N. *et al*. Genomic patterns of progression in smoldering multiple myeloma. *Nat Commun* **9**, 3363, https://doi.org/10.1038/s41467-018-05058-y (2018).
38. Law, E. K. *et al*. The DNA cytosine deaminase APOBEC3B promotes tamoxifen resistance in ER-positive breast cancer. *Science advances* **2**, e1601737, https://doi.org/10.1126/sciadv.1601737 (2016).
39. Yan, S. *et al*. Increased APOBEC3B Predicts Worse Outcomes in Lung Cancer: A Comprehensive Retrospective Study. *J Cancer* **7**, 618–625, https://doi.org/10.7150/jca.14030 (2016).
40. Du, Y. *et al*. APOBEC3B up-regulation independently predicts ovarian cancer prognosis: a cohort study. *Cancer Cell Int* **18**, 78, https://doi.org/10.1186/s12935-018-0572-5 (2018).
41. Nik-Zainal, S. *et al*. Association of a germline copy number polymorphism of APOBEC3A and APOBEC3B with burden of putative APOBEC-dependent mutations in breast cancer. *Nature genetics* **46**, 487–491, https://doi.org/10.1038/ng.2955 (2014).
42. Starrett, G. J. *et al*. The DNA cytosine deaminase APOBEC3H haplotype I likely contributes to breast and lung cancer mutagenesis. *Nat Commun* **7**, 12918, https://doi.org/10.1038/ncomms12918 (2016).
43. Seplyarskiy, V. B. *et al*. APOBEC-induced mutations in human cancers are strongly enriched on the lagging DNA strand during replication. *Genome Res* **26**, 174–182, https://doi.org/10.1101/gr.197046.115 (2016).
44. Hoopes, J. I. *et al*. APOBEC3A and APOBEC3B Preferentially Deaminate the Lagging Strand Template during DNA Replication. *Cell Rep* **14**, 1273–1282, https://doi.org/10.1016/j.celrep.2016.01.021 (2016).
45. Haradhvala, N. J. *et al*. Mutational Strand Asymmetries in Cancer Genomes Reveal Mechanisms of DNA Damage and Repair. *Cell* **164**, 538–549, https://doi.org/10.1016/j.cell.2015.12.050 (2016).
46. Sohail, A., Klapacz, J., Samaranayake, M., Ullah, A. & Bhagwat, A. S. Human activation-induced cytidine deaminase causes transcription-dependent, strand-biased C to U deaminations. *Nucleic acids research* **31**, 2990–2994 (2003).
47. Zeng, X., Negrete, G. A., Kasmer, C., Yang, W. W. & Gearhart, P. J. Absence of DNA polymerase eta reveals targeting of C mutations on the nontranscribed strand in immunoglobulin switch regions. *The Journal of experimental medicine* **199**, 917–924, https://doi.org/10.1084/jem.20032022 (2004).
48. Lindley, R. A. The importance of codon context for understanding the Ig-like somatic hypermutation strand-biased patterns in TP53 mutations in breast cancer. *Cancer genetics* **206**, 222–226, https://doi.org/10.1016/j.cancergen.2013.05.016 (2013).
49. Li, H. & Durbin, R. Fast and accurate short read alignment with Burrows-Wheeler transform. *Bioinformatics (Oxford, England)* **25**, 1754–1760, https://doi.org/10.1093/bioinformatics/btp324 (2009).
50. Li, H. Aligning sequence reads, clone sequences and assembly contigs with BWA-MEM. *arXiv preprint arXiv:1303.3997* (2013).
51. Pleasance, E. D. *et al*. A comprehensive catalogue of somatic mutations from a human cancer genome. *Nature* **463**, 191–196, https://doi.org/10.1038/nature08658 (2010).
52. Pages, V. & Fuchs, R. P. Uncoupling of leading- and lagging-strand DNA replication during lesion bypass *in vivo*. *Science (New York, N.Y.)* **300**, 1300–1303, https://doi.org/10.1126/science.1083964 (2003).
53. Suspene, R. *et al*. Erroneous identification of APOBEC3-edited chromosomal DNA in cancer genomics. *British journal of cancer* **110**, 2615–2622, https://doi.org/10.1038/bjc.2014.176 (2014).
54. Akre, M. K. *et al*. Mutation Processes in 293-Based Clones Overexpressing the DNA Cytosine Deaminase APOBEC3B. *PLoS One* **11**, e0155391, https://doi.org/10.1371/journal.pone.0155391 (2016).
55. An, P. *et al*. APOBEC3B deletion and risk of HIV-1 acquisition. *The Journal of infectious diseases* **200**, 1054–1058, https://doi.org/10.1086/605644 (2009).
56. Yamazaki, H., Tajima, S. & Takeuchi, T. Establishment and characterization of a new human oligosecretory myeloma cell line. *International Journal of Clinical and Experimental Medicine* **9**, 5688–5698 (2016).
57. Murata, M. *et al*. Detecting expressed genes using CAGE. *Methods in molecular biology (Clifton, N.J.)* **1164**, 67–85, https://doi.org/10.1007/978-1-4939-0805-9_7 (2014).
58. Hasegawa, A., Daub, C., Carninci, P., Hayashizaki, Y. & Lassmann, T. MOIRAI: a compact workflow system for CAGE analysis. *BMC bioinformatics* **15**, 144, https://doi.org/10.1186/1471-2105-15-144 (2014).
59. Li, H. *et al*. The Sequence Alignment/Map format and SAMtools. *Bioinformatics (Oxford, England)* **25**, 2078–2079, https://doi.org/10.1093/bioinformatics/btp352 (2009).
60. Consortium, F. *et al*. A promoter-level mammalian expression atlas. *Nature* **507**, 462–470, https://doi.org/10.1038/nature13182 (2014).
61. Salomonis, N. *et al*. Alternative splicing regulates mouse embryonic stem cell pluripotency and differentiation. *Proc Natl Acad Sci USA* **107**, 10514–10519, https://doi.org/10.1073/pnas.0912260107 (2010).
62. Hellman, N. E. *et al*. Matrix metalloproteinase 13 (MMP13) and tissue inhibitor of matrix metalloproteinase 1 (TIMP1), regulated by the MAPK pathway, are both necessary for Madin-Darby canine kidney tubulogenesis. *The Journal of biological chemistry* **283**, 4272–4282, https://doi.org/10.1074/jbc.M708027200 (2008).
63. Eggenschwiler, R. *et al*. Sustained knockdown of a disease-causing gene in patient-specific induced pluripotent stem cells using lentiviral vector-based gene therapy. *Stem cells translational medicine* **2**, 641–654, https://doi.org/10.5966/sctm.2013-0017 (2013).
64. Stenglein, M. D., Burns, M. B., Li, M., Lengyel, J. & Harris, R. S. APOBEC3 proteins mediate the clearance of foreign DNA from human cells. *Nat Struct Mol Biol* **17**, 222–229, https://doi.org/10.1038/nsmb.1744 (2010).
65. Blum, R. *et al*. Intracellular localization and *in vivo* trafficking of p24A and p23. *Journal of cell science* **112**(Pt 4), 537–548 (1999).
66. Kanda, Y. Investigation of the freely available easy-to-use software 'EZR' for medical statistics. *Bone marrow transplantation* **48**, 452–458, https://doi.org/10.1038/bmt.2012.244 (2013).

Acknowledgements

This work was partly supported by Grants-in-Aid for Scientific Research from the Japan Society for the Promotion of Science and research grants from the Ministry of Education, Culture, Sports, Science and Technology (MEXT) of Japan (JP24115004), Japanese Agency for Medical Research and Development (AMED) (JP16fk0410201h0102), the Platform Project for Supporting in Drug Discovery and Life Science Research (Platform for Drug Discovery, Informatics, and Structural Life Science) from AMED (JP16am0101057) and DSK projects to A.T.-K., and by RIKEN Junior Research Associate Program to S.H.

Author Contributions

H.Y., M.K., K.Shirakawa, and A.T.-K. conceived the study; H.Y. carried out experiments with help from T.M., A.D.S., W.M., Y.K., H.M., H.F., K.Shirakawa, K.Shindo; T.M. carried out *in vitro* assays; S.H. and Y.M. analyzed CAGE data; S.I. and M.R. provided patient sample and clinical information, R.S. provided vital reagents; H.Y., K.Shirakawa, and A.T.-K. wrote the paper. All the authors reviewed and approved the manuscript.

Additional Information

Supplementary information accompanies this paper at https://doi.org/10.1038/s41598-019-43575-y.

Competing Interests: The authors declare no competing interests.

Publisher's note: Springer Nature remains neutral with regard to jurisdictional claims in published maps and institutional affiliations.

RESEARCH ARTICLE

APOBEC3B reporter myeloma cell lines identify DNA damage response pathways leading to APOBEC3B expression

Hiroyuki Yamazaki[1], Kotaro Shirakawa[1], Tadahiko Matsumoto[1], Yasuhiro Kazuma[1], Hiroyuki Matsui[1], Yoshihito Horisawa[1], Emani Stanford[1], Anamaria Daniela Sarca[1], Ryutaro Shirakawa[2], Keisuke Shindo[1], Akifumi Takaori-Kondo[1]*

1 Department of Hematology and Oncology, Graduate School of Medicine, Kyoto University, Kyoto, Japan, **2** Department of Molecular and Cellular Biology, Institute of Development, Aging and Cancer, Tohoku University, Sendai, Japan

* atakaori@kuhp.kyoto-u.ac.jp

OPEN ACCESS

Citation: Yamazaki H, Shirakawa K, Matsumoto T, Kazuma Y, Matsui H, Horisawa Y, et al. (2020) APOBEC3B reporter myeloma cell lines identify DNA damage response pathways leading to APOBEC3B expression. PLoS ONE 15(1): e0223463. https://doi.org/10.1371/journal.pone.0223463

Editor: Robert W Sobol, University of South Alabama Mitchell Cancer Institute, UNITED STATES

Received: September 18, 2019

Accepted: December 16, 2019

Published: January 8, 2020

Peer Review History: PLOS recognizes the benefits of transparency in the peer review process; therefore, we enable the publication of all of the content of peer review and author responses alongside final, published articles. The editorial history of this article is available here: https://doi.org/10.1371/journal.pone.0223463

Data Availability Statement: All relevant data are within the manuscript and its Supporting Information files.

Abstract

Apolipoprotein B mRNA-editing enzyme catalytic polypeptide-like (APOBEC) DNA cytosine deaminase 3B (A3B) is a DNA editing enzyme which induces genomic DNA mutations in multiple myeloma and in various other cancers. APOBEC family proteins are highly homologous so it is especially difficult to investigate the biology of specifically A3B in cancer cells. To easily and comprehensively investigate A3B function in myeloma cells, we used CRISPR/Cas9 to generate A3B reporter cells that contain 3×FLAG tag and IRES-EGFP sequences integrated at the end of the A3B gene. These reporter cells stably express 3xFLAG tagged A3B and the reporter EGFP and this expression is enhanced by known stimuli, such as PMA. Conversely, shRNA knockdown of A3B decreased EGFP fluorescence and 3xFLAG tagged A3B protein levels. We screened a series of anticancer treatments using these cell lines and identified that most conventional therapies, such as antimetabolites or radiation, exacerbated endogenous A3B expression, but recent molecular targeted therapeutics, including bortezomib, lenalidomide and elotuzumab, did not. Furthermore, chemical inhibition of ATM, ATR and DNA-PK suppressed EGFP expression upon treatment with antimetabolites. These results suggest that DNA damage triggers A3B expression through ATM, ATR and DNA-PK signaling.

Introduction

The apolipoprotein B mRNA-editing enzyme catalytic polypeptide-like DNA cytosine deaminase 3 family (APOBEC3, A3) consists of seven proteins (A3A, A3B, A3C, A3D, A3F, A3G and A3H) that preferentially induce C to U mutations in single strand DNA. A3 proteins were originally identified as factors of the innate immunity due to their mutagenic activity on viral genomes, and have recently joined the growing list of key intrinsic mutagens that play a part in oncogenesis [1]. Evidence for A3 mutagenicity consists of the presence of their mutational signature in cancer genomes [2], the effects observed when overexpressed in tumor tissues [3, 4],

Funding: This work was partly supported by JSPS KAKENHI Grant numbers JP19H03502, 18H03992 for A.T-K., JP19K07591 for K.S. and by Amedisys Home Health and Hospice Care (AMED) under Grant Number JP19ck0106250, JP19cm0106501 for A.T-K. Research funding from Ono Pharmaceutical Co. for A.T-K. The funders had no role in study design, data collection and analysis, decision to publish, or preparation of the manuscript.

Competing interests: The authors have declared that no competing interests exist.

as well as the correlation of APOBEC signature mutations with poor prognosis [5, 6]. Nevertheless, the precise biology of each APOBEC3 protein in cancer cells remains unknown. Due to the high structural homology of APOBEC3 family members, it is particularly difficult to obtain high-affinity- and high-specificity- antibodies against each APOBEC3 protein, which limits our capability to distinguish the precise role of each endogenous APOBEC3 during tumorigenesis.

Among APOBEC3s, we previously reported that endogenous A3B is overexpressed and seems to be the main source of deamination activity in most of the myeloma cell lines we examined [7]. Notably, high levels of A3B expression in tumor cells were an independent risk factor for the overall survival of myeloma patients [7] as well as of other cancer patients [8–11]. However, the regulatory mechanisms that mediate A3B expression have not been well studied. To date, molecules including cell cycle pathway [12] and DNA damage response (DDR) [13, 14] factors and several transcription factors such as human papillomavirus E6/E7 [15, 16], NF-κB [17, 18], c-Maf [5] and B-Myb [19] were reported to enhance A3B expression. Nevertheless, how these factors mediate A3B expression and how A3B contributes to tumor progression and/or acquisition of chemoresistance in myeloma cells remains unclear. To investigate A3B-associated myeloma biology, we used the CRISPR/Cas9 system to introduce the 3×FLAG tag and the IRES–EGFP gene at the beginning of the 3' UTR of the A3B gene in three human myeloma cell lines. We utilized this reporter cell lines to screen for how A3B expression is affected by anticancer treatments. Overall, we found these reporter cell lines to be very useful for the comprehensive analysis of A3B biology.

Materials and methods

Human cell lines and culture

Three human myeloma cell lines, U266, RPMI8226 and AMO1 cells were maintained in RPMI1640 (Nacalai) containing 10% FBS and 1% PSG (Invitrogen). HEK293T and Lenti-X cells were maintained in DMEM (Nacalai) containing 10% FBS and 1% PSG (Invitrogen).

sgRNA design and construction of A3B reporter donor DNA

To design the single-guide RNA (sgRNA), the mRNA sequence of APOBEC3B (APOBEC3B Homo sapiens chromosome 22, GRCh38 Primary Assembly mRNA variant1, Fig 1A) was imported into CRISPRdirect [20]. After a target site was determined, annealed oligos (S1 Table) were inserted into pSpCas9(BB)–2A–Puro (PX459) V2.0 (Addgene, #62988) using the *BbsI* (New England Biolabs) cloning site, or into lentiCRISPR ver.2 (Addgene, #52961) using the *BsmBI* (New England Biolabs) cloning site as previously described [21, 22]. For the construction of the donor DNA vector (Fig 1B), the right homology arm, the modified cassette including the 3×FLAG–IRES–EGFP gene and the left homology arm were PCR-amplified using KOD FX Neo (ToYoBo). Each PCR primer pair contained around 15 bp overlaps. All the amplicons were cloned into the lentiviral plasmid pCSII–CMV–MCS (RIKEN, RDB04377) by using the In-Fusion HD Cloning Kit (TaKaRa), to produce the pCSII–CMV: A3B–3×FLAG–IRES–EGFP donor DNA plasmid (Fig 1C).

Validation of sgRNA targeting efficiency

293T cells were transfected with pSpCas9(BB)–2A–Puro:sgRNA #4 (0.5 μg) using the FuGENE HD Transfection Reagent (Promega). Two days after transfection, 293T cells were harvested and their genomic DNA extracted using the QuickGene DNA whole blood kit S (KURABO). The targeted region was PCR-amplified from genomic DNA using the targeting test primers

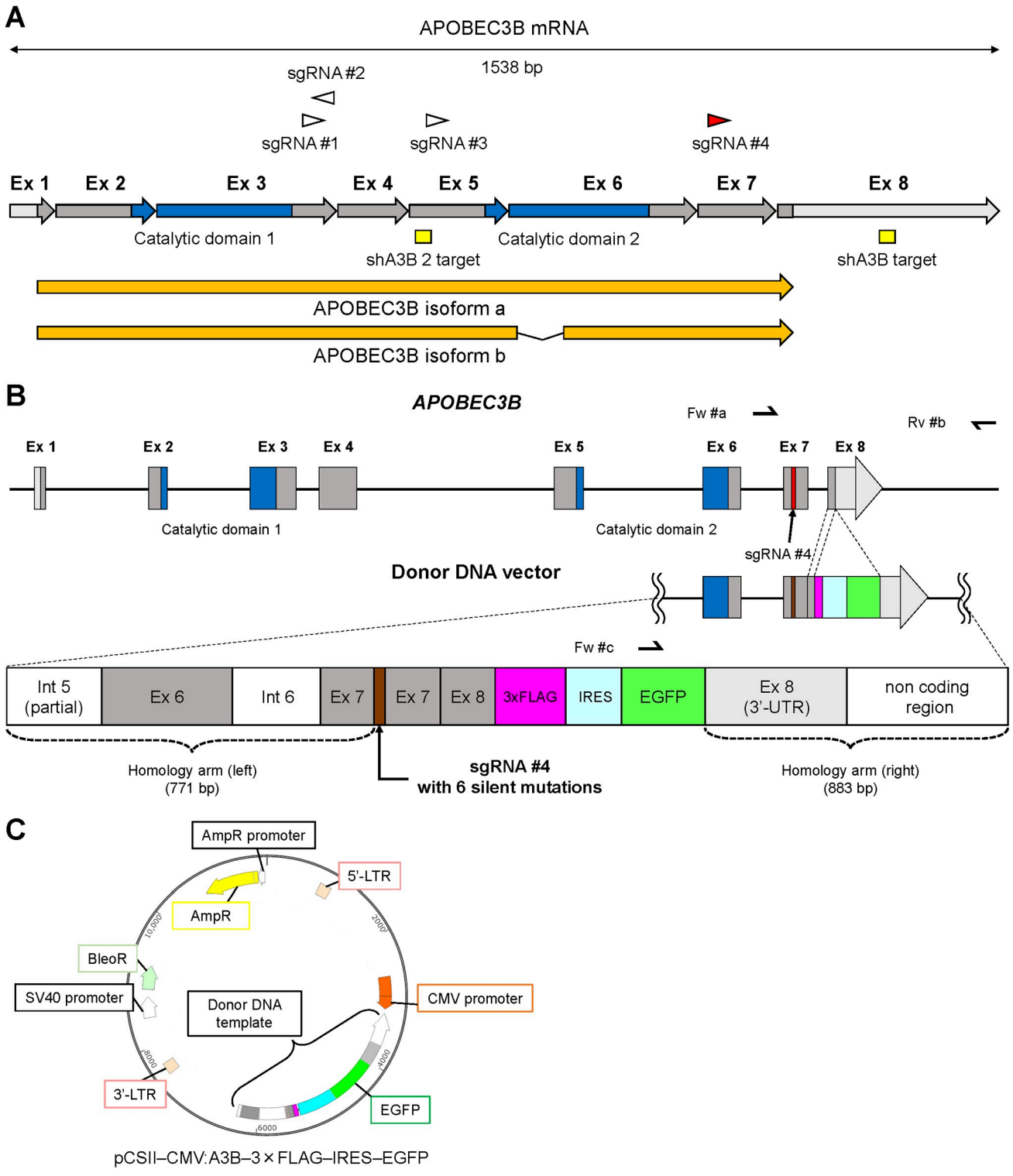

Fig 1. Schema of APOBEC3B editing strategy. (**A**) Schema of A3B mRNA structure. Triangles indicate highly-specific sgRNA target sites within *A3B*. Each arrow represents an exon (Ex). Areas in light gray show UTRs, those in dark gray show coding sequence regions (CDRs), and those in blue show catalytic domains. A3B mRNA isoforms (arrows in orange) as well as shA3B target sites (rectangles in yellow) are also indicated. (**B**) Schema of *A3B* in the host genome and in the donor DNA template. The donor DNA template contains six silent mutations in the sgRNA #4 target site, and intron 7 was removed. The 3×FLAG–IRES–EGFP sequence was inserted adjacent to the beginning of 3' UTR. (**C**) Schema of donor DNA plasmid, pCSII–CMV:A3B–3×FLAG–IRES–EGFP.

https://doi.org/10.1371/journal.pone.0223463.g001

(S1 Table). The PCR products (200 ng) were denatured and then re-annealed to form heteroduplex DNA. The hybridized DNA was digested with T7 endonuclease I (T7E1, New England Biolabs), and run on 2% agarose gel. Mutation frequency was calculated based on band intensity, using Image J software, as previously described [23].

Generation of A3B reporter cell lines

For the U266 and AMO1 cell lines, 5×10^6 cells were co-transfected with 5 μg of pSpCas9 (BB)–2A–Puro:sgRNA #4 plasmid and 5 μg of pCSII–CMV:A3B–3×FLAG–IRES–EGFP donor DNA plasmid using the Amaxa Nucleofector (Lonza) with nucleofection solution R, program X-001. For the RPMI8226 cell line, 5×10^6 cells were transduced with lentiCRISPR ver.2:sgRNA #4 viruses and pCSII–CMV:A3B–3×FLAG–IRES–EGFP donor DNA viruses, simultaneously. These lentiviruses were produced by co-transfection of the packaging plasmid pVSVg (Addgene, #8454), psPAX2-D64V (Addgene, #63586) and lentiCRISPR ver.2:sgRNA #4 plasmid, or pCSII–CMV:A3B–3×FLAG–IRES–EGFP donor DNA plasmid, into Lenti-X cells.

Flow cytometry analysis

Myeloma cells were stained with DRAQ7 (Biostatus) to mark dead cells, then were read on BD FACS Calibur or BD FACS Lyric (Becton-Dickinson Biosciences). To isolate A3B reporter cell lines, EGFP positive cells were sorted using a FACS Aria III cell sorter (Becton-Dickinson Biosciences) at seven days after transfection or transduction. The data was analyzed using the software FCSalyzer ver. 0.9.15-alpha. (https://sourceforge.net/projects/fcsalyzer/).

Genotyping of A3B reporter single cell clones

Single cell clones were isolated from the sorted EGFP-positive cells of the three myeloma cell lines by limiting dilution. These clones were then PCR-genotyped using 2 pairs of the target confirmation primers, forward #a and reverse #b, and forward #c and reverse #b. To confirm the full sequence of A3B–3×FLAG–IRES–EGFP mRNA from the established cell line, complementary DNA (cDNA) was synthesized as described below, and was PCR-amplified by KOD FX Neo (ToYoBo) using a pair of primers, forward #d and reverse #e. The PCR products were sequenced using the 3130xl Genetic Analyzer (Applied Biosystems). All primers for PCR are listed in S1 Table.

Immunoblot analysis

Whole cell lysates from 5.0×10^6 cells, prepared using an SDS-based buffer (5 mM EDTA, 1% SDS) supplemented with Protease inhibitor cocktail (Roche) and PhosSTOP EASY (Roche), were mixed with an equal volume of twofold concentrated sample buffer (Bio-Rad Laboratories) containing β-mercaptoethanol (Nacalai Tesque), and were treated for 5 min at 100˚C. Immunoblot analysis was performed as described previously using a mouse anti-FLAG antibody (Millipore, clone JBW301) or a mouse anti-α-tubulin monoclonal antibody (AA13, Funakoshi).

Immunofluorescence assays

Cells were air-dried and fixed in 4% paraformaldehyde in phosphate-buffered saline (PBS) for 20 minutes on glass slides using Shandon cytospin 2 (THERMO FISHER SCIENTIFIC). Fixed cells were permeabilized, reduced and denatured for 30 minutes in PBS buffer containing 0.5% SDS, 5% β-mercaptoethanol and 10% FBS. Then, cells were washed three times with PBS

containing 4% FBS and 0.1% Triton X-100 (PFT buffer) [24], and incubated with a purified mouse anti-FLAG antibody for 1 hour. Subsequently, cells were incubated with a goat anti-mouse IgG (H+L)-Alexa Flour® 594 preadsorbed antibody (Abcam, ab150120) for 30 min in the dark. All antibodies were diluted with 3% BSA and 0.5% Tween in PBS. Then, the cells were stained with DAPI and were observed with a confocal laser scanning microscope (TCS-SP8, Leica).

Knockdown experiments

We constructed pSicoR-mCherry lentiviral vectors [25] expressing short-hairpin RNA (shRNA) against A3B by inserting synthetic double-stranded oligonucleotides, as previously described [7] (TRCN0000140546 [26], sense oligo, 5′-TGCAAAGCAATGTGCTCCTGATCTCGAGATCAGGAGCACATTGCTTTGCTTTTTTC-3', and antisense oligo, 5′-TCGAGAAAAAAGCAAAGCAATGTGCTCCTGATCTCGAGATCAGGAGCACATTGCTTTGCA-3′; TRCN0000139463, sense oligo, 5′-TCCTGATGGATCCAGACACATTCTCGAGAATGTGTCTGGATCCATCAGGTTTTTTC-3′, and antisense oligo, 5′-TCGAGAAAAAACCTGATGGATCCAGACACATTCTCGAGAATGTGTCTGGATCCATCAGGA-3′) into the cloning site. For non-target shRNA, we used two constructs that were cloned as scrambled sequences (control [27], sense oligo, 5′-TGTCAAGTCTCACTTGCGTCTTCAAGAGAGACGCAAGTGAGACTTGACTTTTTTC-3', antisense oligo, 5′-TCGAGAAAAAAGTCAAGTCTCACTTGCGTCTCTCTTGAAGACGCAAGTGAGACTTGACA-3′; control-2 [28], sense oligo, 5′-TATCTCGCTTGGGCGAGAGTAAGCTCGAGCTTACTCTCGCCCAAGCGAGATTTTTTTC-3′, antisense oligo, 5′-TCGAGAAAAAAATCTCGCTTGGGCGAGAGTAAGCTCGAGCTTACTCTCGCCCAAGCGAGATA). The lentivirus was produced by co-transfection of Trans-Lentiviral packaging plasmid mix (GE Dharmacon) and pSicoR-mCherry into Lenti-X cells.

Quantitative RT-PCR

Total RNA was extracted from cell lines using the High Pure RNA isolation kit (Roche). cDNA was synthesized using the PrimeScriptR II 1st strand cDNA Synthesis Kit (Takara) by random primer and oligo dT primer mixture. Real-time PCR was performed using the Thunderbird SYBR qPCR Mix (ToYoBo). Target gene expression levels were normalized by endogenous expression levels of HPRT1. All primers for real-time PCR are listed in S1 Table.

Anticancer treatment screening

To examine the effects of chemotherapeutic agents on A3B expression, the A3B reporter cells were cultured for two days at a concentration of 2×10^5 cells/well/1.5 mL medium in 12-well plates and treated with phorbol 12-myristate 13-acetate (PMA, Sigma), melphalan (MEL, Wako), cisplatin (CDDP, Nihon-kayaku), mitomycin C (MMC, Funakoshi), N-desacetyl-N-methylocolchicine (COL, KaryoMAX Colcemid Solution in PBS, Thermo Fisher), camptothecin (CPT-11, TopoGEN), etoposide (VP-16, TREVIGEN), cytosine-1-B-D(+)-arabinofuranoside (Ara-C, Wako), gemcitabine hydrochloride (GEM, Sigma), hydroxyurea (HU, Tokyo chemical industry), aphidicolin (APH, Wako), bortezomib (BOR, Funakoshi), lenalidomide (LEN, Sigma), elotuzumab (ELO, Bristol-Myers Squibb), human IFN-α (Sumiferon, Dainippon Sumitomo Pharma) or olaparib (Funakoshi) at several concentrations as described in the main text. These chemotherapeutics were dissolved in 100% dimethyl sulfoxide (Nacalai Tesque) with the exception of COL, HU, ELO and INF-α which were dissolved in distilled water. To examine the effects of radiation or UV on A3B expression, the cells were exposed to gamma radiation using a Cs-137 Gamma Cell or to UVC using a FUNA UV Crosslinker, FS-800 (Funakoshi). To examine the effects of kinase inhibitors on A3B regulation, KU-55933

(Selleck), VE-821 (Selleck), NU-7026 (Selleck) or CGK733 (Calbiochem) were added 2 hours prior to antimetabolite treatment.

Statistical analysis

Mann-Whitney U test and Welch's t test were calculated to evaluate the differences in continuous variables between two groups for quantitative RT-PCR results and flow cytometry results, respectively, by using the EZR software (version 3.0.2, Saitama Medical Center, Jichi Medical University) [29].

Results

CRISPR design

We first designed sgRNA candidates for target sites in *A3B*, excluding introns, using the web based tool, CRISPRdirect [20]. There are only four highly specific candidates for *A3B* (Fig 1A and S2 Table) mainly due to the high homology among APOBEC3 family genes. In order to insert the 3×FLAG sequence into *A3B* with a minimal off-target effect, we selected sgRNA #4 (Fig 1A). U266, RPMI8266 and AMO1 endogenously overexpress *A3B* [7]. We used the pSpCas9(BB)–2A–Puro plasmid and the lentiCRISPR ver.2 plasmid to transduce the CRISPR system that targets *APOBEC3B* loci in these cell lines. We also used a donor DNA template to introduce the 3×FLAG and IRES-EGFP reporter sequences at the end of the coding region and to move the stop codon behind the 3×FLAG sequence (Fig 1B and 1C). The 3×FLAG–IRES–EGFP cassette was located adjacent to the beginning of 3' UTR, and intron 7 (281bp) was removed to prevent it from becoming the right homology arm. Usually, the PAM sequence (NGG) in the donor DNA template must be mutated to prevent cutting by Cas9, however, in our case, any mutation of PAM would lead to alteration of the A3B protein sequence. Instead, we designed six silent mutations within the target site to inhibit efficient future sgRNA binding: the host genomic target sequence of sgRNA #4, 'ctgGGACACCTTTG TGTACCGCCAGGgat', was altered to 'ctgGGACACGTTCGTCTATCGACAAGgat', in the donor DNA template sequence. Finally, the complete donor DNA template sequence was inserted into the pCSII–CMV–MCS plasmid in the opposite direction of the CMV promoter of the parental vector (Fig 1C), so that cells in which the donor DNA vector is present merely transiently would not express *EGFP* and only cells which had their genome successfully engineered would emit EGFP fluorescent signals.

CRISPR guided 3×FLAG–IRES–EGFP insertion in *A3B* locus

To test the targeting efficiency of the sgRNA, we transfected the pSpCas9(BB)–2A–Puro: sgRNA #4 plasmid into 293T cells. The transfection efficiency was 15.2% (T7E1 assay, Fig 2A), therefore, we proceeded to co-transfect/co-transduce Cas9, the sgRNA #4 expressing vector and the donor DNA vector into U266, RPMI8226 and AMO1 cell lines. As expected, the efficiency of genome editing in myeloma cells was quite low, but we successfully enriched EGFP positive cells by cell sorting (Fig 2B). Single clones were isolated by limiting dilution from each cell line, expanded and A3B genotype was confirmed by PCR. Out of all the isolated clones, we selected the following four edited cell lines: U266$^{A3B–3×FLAG–IRES–EGFP}$ #1 and #2 (U266 KI #1 and #2), RPMI8226$^{A3B–3×FLAG–IRES–EGFP}$ (RPMI8226 KI), and AMO1$^{A3B–3×FLAG–IRES–EGFP}$ (AMO1 KI). According to the genotype PCR in Fig 2C, the A3B–3×FLAG–IRES–EGFP cassette was correctly integrated at the target site in these cell lines. Of note, both A3B alleles in U266 KI #2 were edited (Fig 2C). To confirm the mRNA sequence of A3B–3×FLAG–IRES–EGFP, we PCR-amplified the full length of the cDNA derived from each cell line (Fig 2D) and

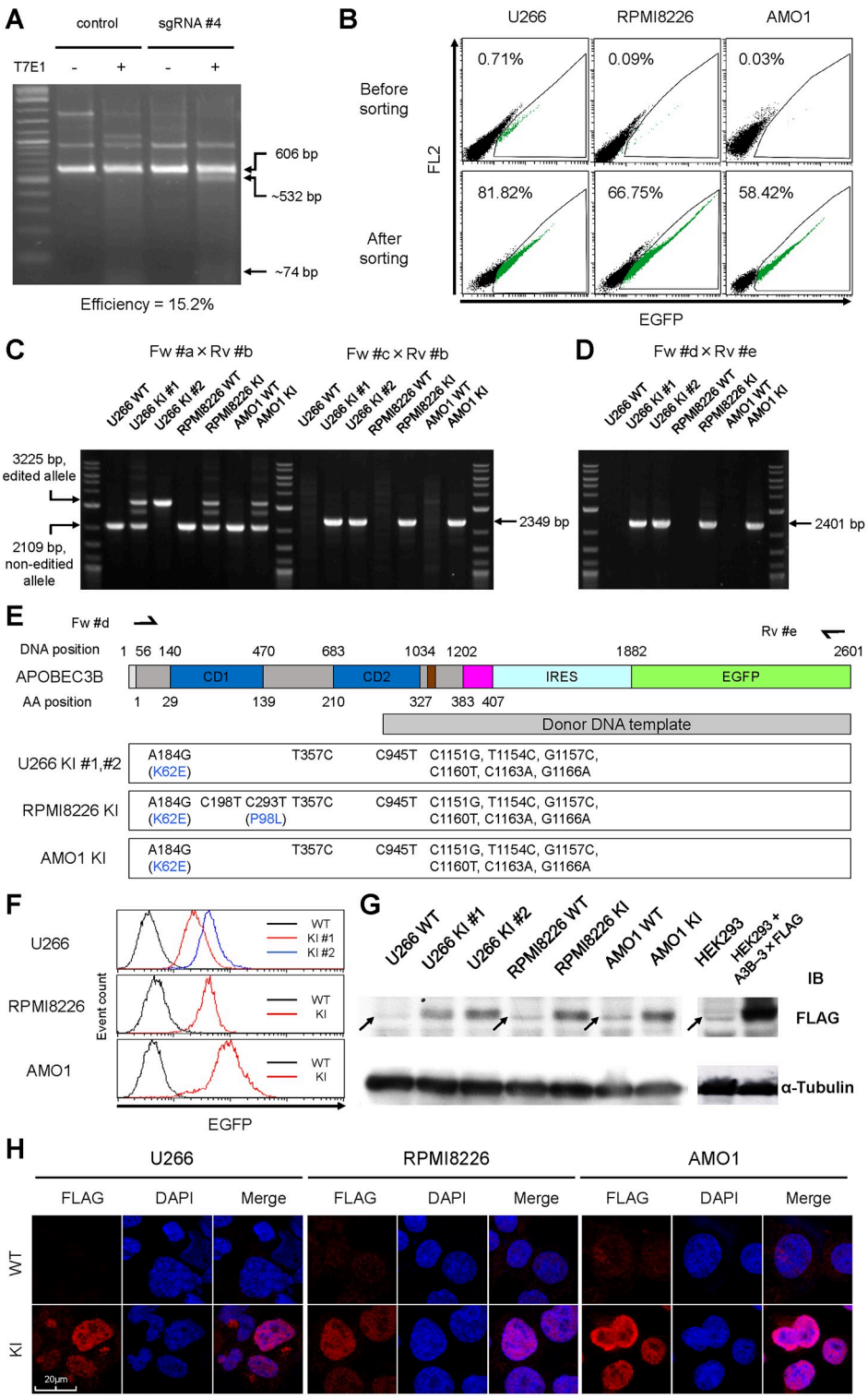

Fig 2. Establishment of A3B–3×FLAG–IRES–EGFP knock-in myeloma cell lines. (**A**) T7E1 assay of the sgRNA #4 site in 293T cells. Expected positions of uncleaved (606 bp) and cleaved (532 bp and 74 bp) DNA bands by T7E1 are indicated with arrows. The mutation frequency is also shown. (**B**) Flow cytometry of U266, RPMI8226 and AMO1 cells after introducing the donor DNA vector along with the CRISPR-Cas9 vector. EGFP positive cells are highlighted in green and their proportions are indicated. (**C**) Genotyping PCR of genomic DNA from each clone derived from a single cell among the enriched cells in (B). Each clone was genotyped by two pairs of primers, Fw #a × Rv #b and Fw

#c × Rv #b. Using the former primer pair, the expected size of the PCR amplicon is 2109 bp for the wild type allele, and 3225 bp for the knock-in allele. Using the latter primer pair, the PCR amplicon (2349 bp) can be detected only if the knock-in allele is present. (**D**) Genotyping PCR of cDNA from each clone in (C). The PCR amplicon (2401 bp) can be detected only if the knock-in allele is present. (**E**) Sanger sequencing results for the full length of the edited A3B cDNA originated from the clones of 3×FLAG–IRES–EGFP knock-in cell lines. Schema of the A3B–3×FLAG–IRES–EGFP mRNA structure is also depicted, the same as in Fig 1B. (**F**) Histograms of EGFP intensity values from the 3×FLAG–IRES–EGFP knock-in cell lines as determined by flow cytometry. (**G**) Immunoblot analysis of the 3×FLAG–IRES–EGFP knock-in cell lines. Lysates of untransduced HEK293 and A3B–3×FLAG overexpressing HEK293 were also blotted as negative and positive control, respectively. Arrows indicate non-specific bands. α-tubulin was evaluated as internal control. (**H**) Immunofluorescence analysis of the 3×FLAG–IRES–EGFP knock-in clones using an anti-FLAG antibody. For U226 KI, clone U266 KI #1 was examined. Images were obtained by confocal fluorescence microscopy (magnification, x630).

https://doi.org/10.1371/journal.pone.0223463.g002

performed Sanger sequencing analysis. As desired, all the engineered cell lines possessed correct A3B–3×FLAG sequences, including the intended 6 silent mutations in the sgRNA target site and SNPs in the unmanipulated region (Fig 2E). According to flow cytometry analysis, the intensity of the fluorescent signal increased in the order of U266 KI #1, RPMI8226 KI and AMO1 KI, which is consistent with their A3B expression levels in a previous report [7]. U266 KI #2 exhibited around two times stronger fluorescence than U266 KI #1, indicating that the 3×FLAG–IRES–EGFP gene was integrated homozygously in U266 KI #2 and heterozygously in U266 KI #1. According to the results of flow cytometry and PCR-genotyping (Fig 2C), RPMI8226 KI and AMO1 KI contain a single allele of the 3×FLAG–IRES–EGFP gene. Immunoblot analysis also confirmed that all the cell lines produced A3B–3×FLAG proteins of the predicted size (Fig 2G). Immunofluorescent analysis of the subcellular localization of A3B–3×FLAG proteins showed a dominant localization in the nucleoplasm (Fig 2H), which is identical with that of wild type A3B proteins [7].

The established A3B–3×FLAG–IRES–EGFP knock-in cell lines work as A3B reporters

To verify the feasibility of the established cell lines as A3B reporters, we first transduced RPMI8226 KI and AMO KI cells with lentiviral shRNA against A3B together with an EF1α-driven mCherry fluorescent marker. When A3B mRNA was efficiently depleted (Fig 3A), A3B–3×FLAG protein levels decreased as expected (Fig 3B). Similarly, EGFP fluorescence intensity decreased in mCherry positive, shRNA transduced cells, compared with mCherry negative, shRNA non-transduced cells (Fig 3C–3F). Next, we treated U266 KI #1, RPMI8226 KI and AMO1 KI cells with PMA, a PKC activator, which is known to upregulate A3B expression via the NF-κB pathway [17, 18]. A quantitative RT-PCR analysis confirmed the enhancement of A3B mRNA levels for each cell line (Fig 3G). Consistently, immunoblot analysis detects increases of A3B–3×FLAG proteins (Fig 3H), and flow cytometry analysis detects peak shifts and increases of mean fluorescent intensity (MFI) for each cell line (Fig 3I and 3J). Based on the above results, we conclude that these established cell lines can be used as reliable A3B reporters.

DDR upregulates A3B expression via all the DDR-PIKK pathways in myeloma cells

Because the established A3B reporter cell lines provide an easy way to evaluate the alteration of A3B expression by simply performing flow cytometry analysis, we investigated which of the current clinically approved myeloma treatments affect A3B expression. Interestingly, most conventional anticancer treatments which induce DNA interstrand cross-links (e.g., CDDP, MEL and MMC), microtubule inhibition (e.g.,COL), topoisomerase inhibition (e.g.,CPT-11

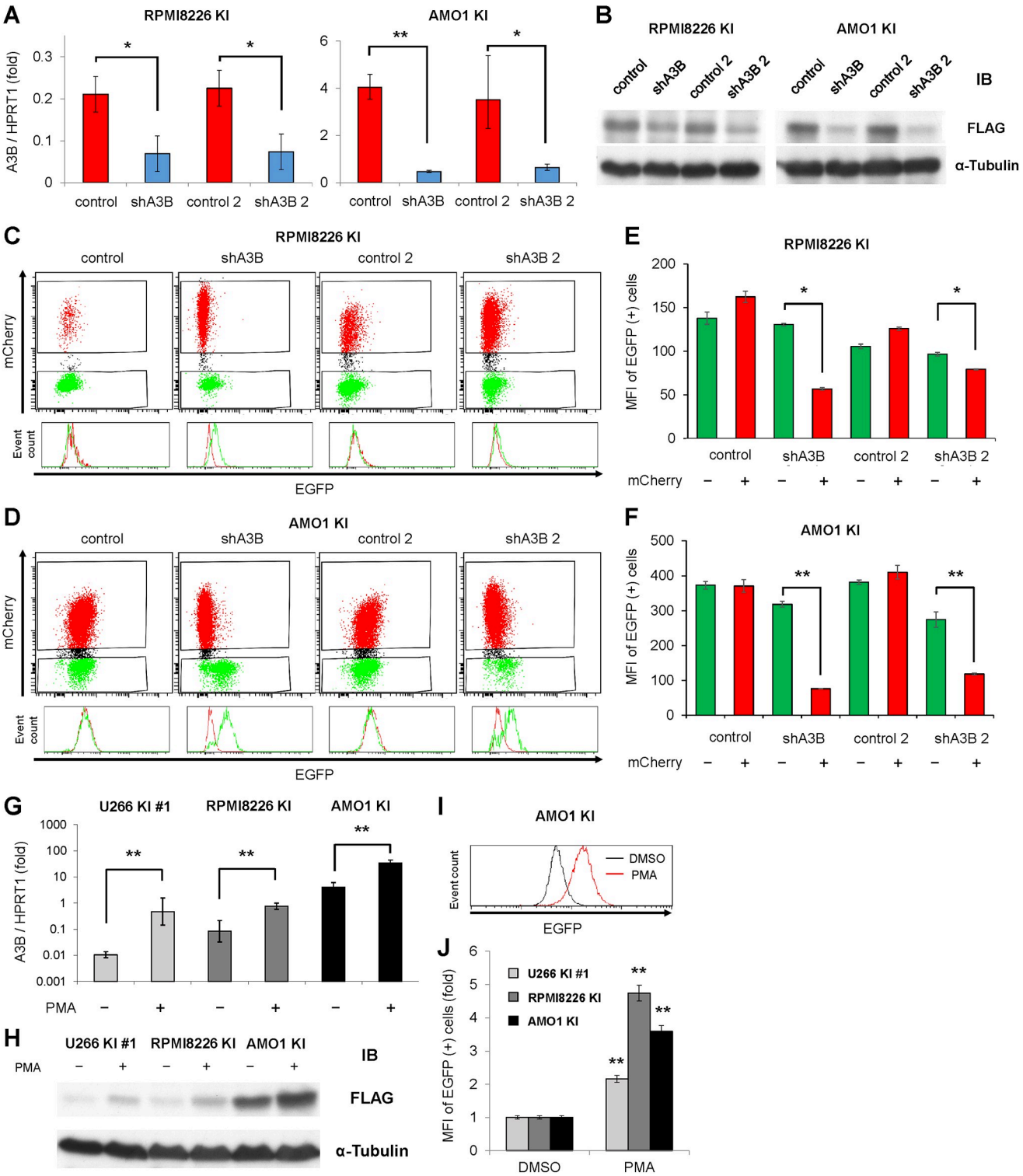

Fig 3. A3B–3×FLAG–IRES–EGFP knock-in cells work as A3B reporters. (**A**, **B**) Real-time PCR (A) and immunoblotting (B) of A3B in RPMI8226 KI cells and AMO1 KI cells, which were transduced with lentiviral shRNA against A3B (two constructs: shA3B or shA3B-2) or control (two constructs: control or control-2). HPRT1 or α-tubulin were evaluated as internal controls. Mann-Whitney U tests were used to compare the results between control and A3B knockdown samples: $^{**}P < 0.01$; $^{*}P < 0.05$. (**C**, **D**) Flow cytometry of RPMI8226 KI cells (C) and AMO1 KI cells (D) at 17 days after transduction with lentiviral shRNA against A3B or control. In the histogram representation, EGFP intensity was compared between mCherry positive cells (colored in red) and mCherry negative cells (colored in green). (**E**, **F**) Bar graph of EGFP mean fluorescence intensity (MFI) of the experiments in Figures (C, D).

Mann-Whitney U tests were performed to compare the results between mCherry negative and mCherry positive samples: $^{**}P < 0.01$; $^{*}P < 0.05$. (**G**, **H**) Real-time PCR (G) and immunoblotting (H) of A3B in three A3B–3×FLAG–IRES–EGFP knock-in cell lines, which were treated with PMA (20 ng/mL) for 6 hours and 24 hours, respectively. Mann-Whitney U tests were performed to compare the results between control and PMA-treated samples: $^{**}P < 0.01$. (**I**) Representative result of EGFP intensity histogram of AMO1 KI cells, which were treated with PMA (20 ng/mL) for 2 days. (**J**) Bar graph of EGFP mean fluorescent intensity (MFI) of three A3B–3×FLAG–IRES–EGFP knock-in cell lines, which were treated with PMA (20 ng/mL) for 2 days. Mann-Whitney U tests were performed to compare the results between control and PMA-treated samples: $^{**}P < 0.01$.

https://doi.org/10.1371/journal.pone.0223463.g003

and VP-16), DNA synthesis inhibition (e.g., Ara-C, GEM, HU and aphidicolin) or DNA double-strand breaks (e.g., radiation), exacerbated endogenous A3B overexpression (Fig 4A and 4B). Treatment with olaparib alone, a Poly(ADP-ribose) polymerase (PARP) inhibitor, which is known to induce SSBs that are degraded to DSBs during replication [30], also enhanced A3B expression (Fig 4C). On the other hand, the proteasome inhibitor (i.e., BOR), the immunomodulatory drug (i.e., LEN), the non-agonistic antibody drug (i.e., ELO) and INF-α did not enhance A3B expression levels (Fig 4A). These results intimate that DNA toxic stimulation upregulates A3B expression through DDR and following activation of DDR associated phosphatidylinositol 3' kinase-related kinases (DDR-PIKKs) [31] including ataxia telangiectasia and Rad3-related (ATR), and ataxia telangiectasia-mutated (ATM), DNA-dependent protein kinase (DNA-PK). Chemical inhibition of DDR-PIKKs by VE-821 for ATR, or NU-7026 for DNA-PK, suppressed EGFP increase upon antimetabolite treatment (Fig 4D and 4E). Moreover, various combinations of PIKK inhibitors, including KU-55933, an ATM inhibitor, exhibited a synergistic effect of preventing A3B expression increase upon antimetabolite stimulation (Fig 4D and 4E). Notably, pretreatment with CGK733 alone, which was first reported as an ATM/ATR inhibitor [32], almost completely blocked the antimetabolite effect on A3B expression in the three cell lines (Fig 4F). These results suggest that all the DDR-PIKK pathways might be involved in A3B regulation in myeloma cells.

Discussion

In the present report, we successfully established four A3B reporter cell lines derived from three human myeloma cell lines, U266, RPMI8226 and AMO1. These cell lines express EGFP proteins with attribution to A3B expression, regulated by the same transcriptional/posttranscriptional mechanisms due to identical promoter, 3'-UTR and 5'-UTR to *A3B*. Due to these particularities, these cell lines are a very useful tool for investigating A3B regulation in a high-throughput screening format by flow cytometry analysis, which will allow for the development of specific A3B suppressors. There are several similar reports of other gene-edited reporter cell lines used for comprehensively studying the transcriptional regulation of the targeted gene [33–37]. In the case of A3B, most previous reports have studied A3B protein function using exogenous overexpression by transient transfection in a limited number of cell lines including non-human cells [16, 26, 38–44], mainly due to the difficulty of obtaining specific anti-A3B antibodies. In contrast, the commercially available and certified anti-FLAG antibody can be used to explore the A3B protein in the established A3B reporter cell lines described here. That is to say, these cell lines have the potential to clarify natural protein-protein and/or DNA-protein interaction of A3B specifically, in tumor cells. In addition, the A3B reporter system can be integrated into other A3B-overexpressing cell lines by using the Cas9/sgRNA #4 expressing vector and pCSII–CMV:A3B–3×FLAG–IRES–EGFP donor DNA vector described here.

According to our pilot screening, most of the conventional anticancer treatments exacerbated A3B overexpression in myeloma cells (Fig 4A and 4B). These treatments seem to act through a common pathway: induction of DDR [45]. Specifically, HU, which inhibits the incorporation of nucleotides by interfering with the enzyme ribonucleotide reductase [46], and APH, which interferes with DNA replication by inhibiting DNA polymerases α, ε and δ

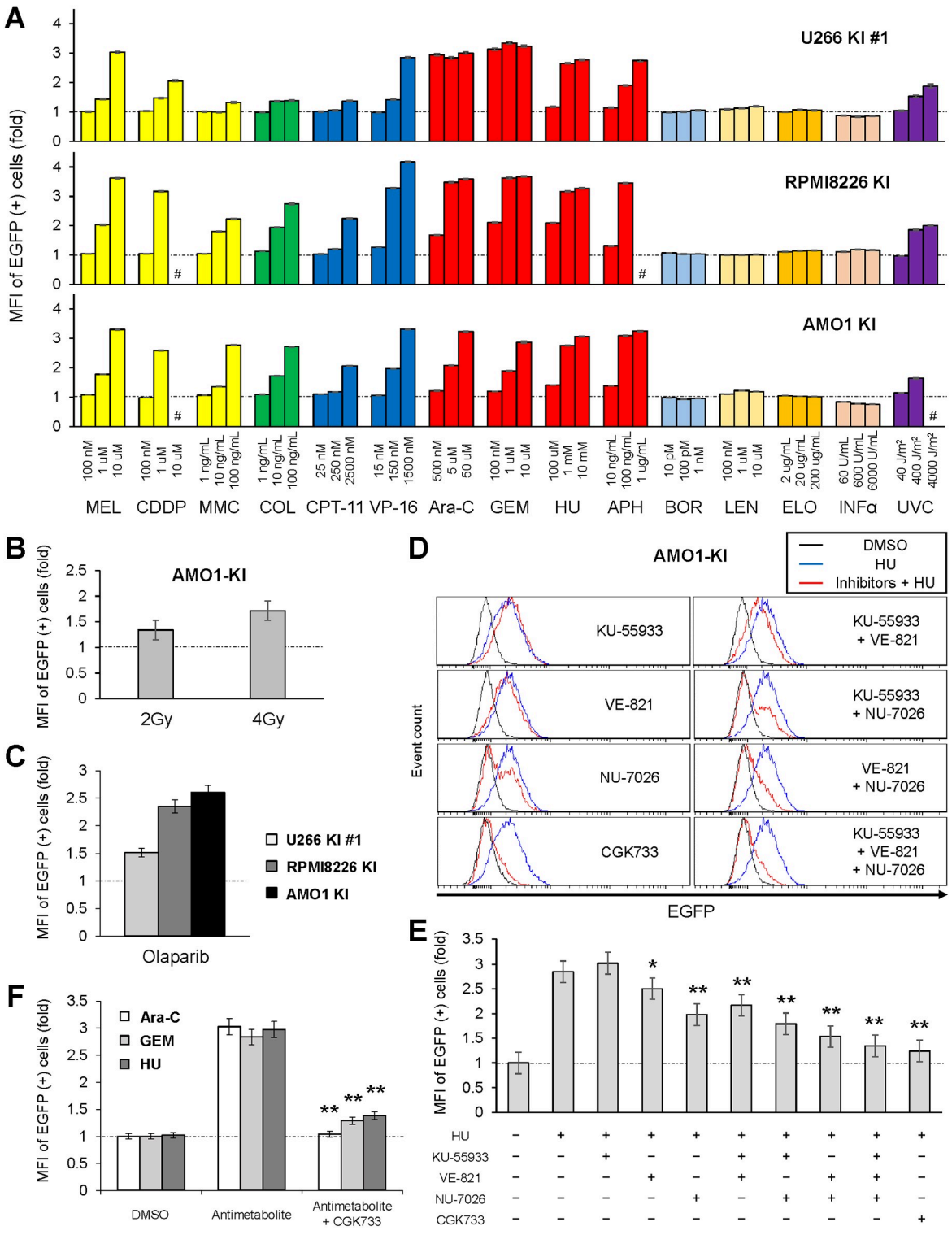

Fig 4. DNA damage response exacerbates A3B overexpression via the DDR-PIKK pathways in myeloma cells. (**A**) A panel of EGFP mean fluorescent intensity (MFI) of three A3B–3×FLAG–IRES–EGFP knock-in cell lines with various anti-cancer treatment. A3B reporter cells were incubated for 2 days with each anti-cancer reagent at the concentrations indicated on the horizontal axis. For the UVC exposure experiment, A3B reporter cells were irradiated with a single dose at 2 days before flow cytometry analysis. Hash mark (#) represents unmeasurable state due to cytotoxicity. (**B**) Bar graph of EGFP MFI of AMO1 KI cells, which were exposed to a single dose of γ-ray at 2 days before flow cytometry analysis. (**C**) Bar graph of EGFP MFI of three A3B–3×FLAG–IRES–EGFP knock-in cell lines with

olaparib treatment (10 μM) for 2 days. (**D**, **E**) Histograms (D) and bar graphs (E) of EGFP intensity values from AMO1 KI cells, which were co-treated with HU (1μM) and DDR-PIKK inhibitors: KU-55933, 5 μM; VE-821, 5 μM; NU-7026, 2 μM; CGK733, 5 μM. Cells were incubated with the reagents for 2 days and subsequently analyzed by flow cytometry. Mann-Whitney U tests were performed to compare the results between HU-treated and PIKK inhibitor-treated samples: $^{**}P < 0.01$; $^{*}P < 0.05$. (**F**) Bar graph of EGFP MFI of three A3B–3×FLAG–IRES–EGFP knock-in cell lines treated with an antimetabolite (Ara-C, 50 μM; GEM, 1 μM; HU, 1 μM) with or without CGK733 (5 μM) for 2 days. Mann-Whitney U tests were performed to compare the results between antimetabolite-treated and CGK733-treated sample: $^{**}P < 0.01$.

https://doi.org/10.1371/journal.pone.0223463.g004

[47], are both commonly used to induce replication fork stalling that leads to ATR/ATM activation. These antimetabolites are also known to induce DSBs [48, 49]. CPT-11 covalently stabilizes the topoisomerase I–DNA cleavage complex by inhibiting the ligation of SSBs [50], thereby increasing the number of SSBs and subsequent DSBs [51]. Meanwhile, VP-16 leads to increases in the levels of topoisomerase II–DNA covalent complexes resulting in the rapid induction of DSBs [52]. DNA interstrand cross-linkers form a number of adducts with DNA, and thereafter activate a wide variety of DNA repair pathways [53] such as nucleotide excision repair (NER) [54, 55], homology-directed repair (HDR) [56] and mismatch repair (MMR) [57]. DNA interstrand cross-links are also known to be sensed by non-histone chromosomal high-mobility group box proteins 1 and 2 (HMGB1 and HMGB2), which affect cell cycle events and subsequently induce apoptosis [58]. Colcemid also has the potential to induce DSBs [59, 60]. Although UV exposure dominantly produces cyclobutane pyrimidine dimers (CPDs) and 6–4 photoproducts (6-4PP) but not DSBs directly, it activates ATR by SSBs and ATM by DSBs in a NER-dependent manner [61]. On the other hand, bortezomib and lenalidomide did not enhance A3B overexpression (Fig 4A). We cannot exclude the possibility that these drugs can directly cause DSBs, however, there are few reports of DNA damage induced by a single treatment with bortezomib or lenalidomide.

The upregulation of A3B expression induced by DNA damage was suppressed by DDR-PIKK inhibitors, consistent with a previous report in breast cancer [13]. Under single-inhibition of each DDR-PIKK pathway, the DNA-PK inhibitor (NU-7026) suppressed A3B elevation the strongest. Kanu et al. reported that inhibiting ATR, and to a lesser extent ATM, reduced hydroxyurea-induced A3B activation, and concluded that DNA replication stress activates transcription of A3B via an ATR/Chk1-dependent pathway in breast cancer [13]. Thus, the dependency of A3B regulation on each DDR-PIKK pathway could vary among cancer cell types. On closer examination of the histograms in our study, EGFP signal curves from cells treated with NU-7026 had two peaks in contrast to those treated with VE-821 which had only one peak (Fig 4D), suggesting that DNA-PK inhibition completely blocked A3B upregulation in a certain population of cells, whereas ATR inhibition suppressed it in all cells. Considering the synergistic effects of the combinations of DDR-PIKK inhibitors in our study (Fig 4D and 4E), it seems that all the DDR-PIKK pathways are at least partly involved in A3B regulation in myeloma cells. This model is also supported by the redundancy between DDR-PIKK pathways under DNA replication stress [62]. Interestingly, A3B induction by DDR was almost completely blocked by treatment with CGK733 alone. CGK733 was initially reported to inhibit both ATM and ATR kinase activities, however, its specificity is now considered controversial [63, 64]. Nonetheless, there seems to be no doubt that CGK733 targets at least partly a downstream factor of the ATM/ATR pathway [65, 66]. HMGB1 and Cdc7 were identified as new target kinase candidates of CGK733 [67]. Of note, proteasome inhibitors were reported to suppress DDR by inhibiting phosphorylation of DDR-PIKKs [68, 69]. This suppression effect could explain why bortezomib did not exacerbate A3B expression.

We previously reported that shRNA against A3B decreased the basal level of γH2AX foci in myeloma cell lines, indicating that A3B induces constitutive DNA double-strand breaks,

promoting DDR activation [7]. Therefore DDR-inducible treatments trigger a positive feedback loop for A3B expression, which may drive chemoresistant clone expansion during chemotherapy. To prevent disease progression and potentiate current therapy, conventional anticancer treatment coupled with a combination of DDR-PIKK inhibitors including a proteasome inhibitor might not only have a synergistic cytotoxicity for tumor cells but also suppress the production of chemoresistant clones.

Supporting information

S1 Fig. Original membranes and gels.
(PDF)

S1 Table. List of oligos and thermal cycle conditions for genotyping PCR.
(XLSX)

S2 Table. sgRNA target candidates for A3B.
(XLSX)

Acknowledgments

Plasmids including pSpCas9(BB)–2A–Puro (PX459) V2.0 (#62988), lentiCRISPR ver.2 (#52961), pVSVg (#8454), psPAX2-D64V (#63586) were provided by Addgene.

Author Contributions

Conceptualization: Hiroyuki Yamazaki, Kotaro Shirakawa, Akifumi Takaori-Kondo.

Funding acquisition: Kotaro Shirakawa, Akifumi Takaori-Kondo.

Investigation: Hiroyuki Yamazaki, Kotaro Shirakawa, Tadahiko Matsumoto, Yasuhiro Kazuma, Hiroyuki Matsui, Yoshihito Horisawa, Emani Stanford, Anamaria Daniela Sarca, Keisuke Shindo.

Methodology: Hiroyuki Yamazaki, Ryutaro Shirakawa.

Resources: Hiroyuki Yamazaki, Ryutaro Shirakawa.

Supervision: Kotaro Shirakawa, Akifumi Takaori-Kondo.

Validation: Akifumi Takaori-Kondo.

Writing – original draft: Hiroyuki Yamazaki, Kotaro Shirakawa.

Writing – review & editing: Hiroyuki Yamazaki, Kotaro Shirakawa, Tadahiko Matsumoto, Yasuhiro Kazuma, Hiroyuki Matsui, Yoshihito Horisawa, Emani Stanford, Anamaria Daniela Sarca, Keisuke Shindo, Akifumi Takaori-Kondo.

References

1. Henderson S, Fenton T. APOBEC3 genes: retroviral restriction factors to cancer drivers. Trends in molecular medicine. 2015; 21(5):274–84. https://doi.org/10.1016/j.molmed.2015.02.007 PMID: 25820175
2. Alexandrov LB, Nik-Zainal S, Wedge DC, Aparicio SA, Behjati S, Biankin AV, et al. Signatures of mutational processes in human cancer. Nature. 2013; 500(7463):415–21. https://doi.org/10.1038/nature12477 PMID: 23945592
3. Swanton C, McGranahan N, Starrett GJ, Harris RS. APOBEC Enzymes: Mutagenic Fuel for Cancer Evolution and Heterogeneity. Cancer Discov. 2015; 5(7):704–12. https://doi.org/10.1158/2159-8290.CD-15-0344 PMID: 26091828

4. Gao J, Choudhry H, Cao W. Apolipoprotein B mRNA editing enzyme catalytic polypeptide-like family genes activation and regulation during tumorigenesis. Cancer science. 2018; 109(8):2375–82. https://doi.org/10.1111/cas.13658 PMID: 29856501
5. Walker BA, Wardell CP, Murison A, Boyle EM, Begum DB, Dahir NM, et al. APOBEC family mutational signatures are associated with poor prognosis translocations in multiple myeloma. Nat Commun. 2015; 6:6997. https://doi.org/10.1038/ncomms7997 PMID: 25904160
6. Maura F, Petljak M, Lionetti M, Cifola I, Liang W, Pinatel E, et al. Biological and prognostic impact of APOBEC-induced mutations in the spectrum of plasma cell dyscrasias and multiple myeloma cell lines. Leukemia. 2018; 32(4):1044–8. https://doi.org/10.1038/leu.2017.345 PMID: 29209044
7. Yamazaki H, Shirakawa K, Matsumoto T, Hirabayashi S, Murakawa Y, Kobayashi M, et al. Endogenous APOBEC3B Overexpression Constitutively Generates DNA Substitutions and Deletions in Myeloma Cells. Scientific reports. 2019; 9(1).
8. Sieuwerts AM, Willis S, Burns MB, Look MP, Meijer-Van Gelder ME, Schlicker A, et al. Elevated APOBEC3B correlates with poor outcomes for estrogen-receptor-positive breast cancers. Hormones & cancer. 2014; 5(6):405–13.
9. Law EK, Sieuwerts AM, LaPara K, Leonard B, Starrett GJ, Molan AM, et al. The DNA cytosine deaminase APOBEC3B promotes tamoxifen resistance in ER-positive breast cancer. Science advances. 2016; 2(10):e1601737. https://doi.org/10.1126/sciadv.1601737 PMID: 27730215
10. Yan S, He F, Gao B, Wu H, Li M, Huang L, et al. Increased APOBEC3B Predicts Worse Outcomes in Lung Cancer: A Comprehensive Retrospective Study. J Cancer. 2016; 7(6):618–25. https://doi.org/10.7150/jca.14030 PMID: 27076842
11. Du Y, Tao X, Wu J, Yu H, Yu Y, Zhao H. APOBEC3B up-regulation independently predicts ovarian cancer prognosis: a cohort study. Cancer Cell Int. 2018; 18:78. https://doi.org/10.1186/s12935-018-0572-5 PMID: 29853799
12. Ng JCF, Quist J, Grigoriadis A, Malim MH, Fraternali F. Pan-cancer transcriptomic analysis dissects immune and proliferative functions of APOBEC3 cytidine deaminases. Nucleic acids research. 2019.
13. Kanu N, Cerone MA, Goh G, Zalmas LP, Bartkova J, Dietzen M, et al. DNA replication stress mediates APOBEC3 family mutagenesis in breast cancer. Genome biology. 2016; 17(1):185. https://doi.org/10.1186/s13059-016-1042-9 PMID: 27634334
14. Shimizu A, Fujimori H, Minakawa Y, Matsuno Y, Hyodo M, Murakami Y, et al. Onset of deaminase APOBEC3B induction in response to DNA double-strand breaks. Biochem Biophys Rep. 2018; 16:115–21. https://doi.org/10.1016/j.bbrep.2018.10.010 PMID: 30417129
15. Vieira VC, Leonard B, White EA, Starrett GJ, Temiz NA, Lorenz LD, et al. Human papillomavirus E6 triggers upregulation of the antiviral and cancer genomic DNA deaminase APOBEC3B. mBio. 2014; 5(6).
16. Mori S, Takeuchi T, Ishii Y, Kukimoto I. Identification of APOBEC3B promoter elements responsible for activation by human papillomavirus type 16 E6. Biochem Biophys Res Commun. 2015; 460(3):555–60. https://doi.org/10.1016/j.bbrc.2015.03.068 PMID: 25800874
17. Leonard B, McCann JL, Starrett GJ, Kosyakovsky L, Luengas EM, Molan AM, et al. The PKC/NF-kappaB signaling pathway induces APOBEC3B expression in multiple human cancers. Cancer Res. 2015; 75(21):4538–47. https://doi.org/10.1158/0008-5472.CAN-15-2171-T PMID: 26420215
18. Maruyama W, Shirakawa K, Matsui H, Matsumoto T, Yamazaki H, Sarca AD, et al. Classical NF-kappaB pathway is responsible for APOBEC3B expression in cancer cells. Biochem Biophys Res Commun. 2016; 478(3):1466–71. https://doi.org/10.1016/j.bbrc.2016.08.148 PMID: 27577680
19. Chou WC, Chen WT, Hsiung CN, Hu LY, Yu JC, Hsu HM, et al. B-Myb Induces APOBEC3B Expression Leading to Somatic Mutation in Multiple Cancers. Scientific reports. 2017; 7:44089. https://doi.org/10.1038/srep44089 PMID: 28276478
20. Naito Y, Hino K, Bono H, Ui-Tei K. CRISPRdirect: software for designing CRISPR/Cas guide RNA with reduced off-target sites. Bioinformatics (Oxford, England). 2015; 31(7):1120–3.
21. Ran FA, Hsu PD, Wright J, Agarwala V, Scott DA, Zhang F. Genome engineering using the CRISPR-Cas9 system. Nature protocols. 2013; 8(11):2281–308. https://doi.org/10.1038/nprot.2013.143 PMID: 24157548
22. Shalem O, Sanjana NE, Hartenian E, Shi X, Scott DA, Mikkelson T, et al. Genome-scale CRISPR-Cas9 knockout screening in human cells. Science (New York, NY). 2014; 343(6166):84–7.
23. Guschin DY, Waite AJ, Katibah GE, Miller JC, Holmes MC, Rebar EJ. A rapid and general assay for monitoring endogenous gene modification. Methods in molecular biology (Clifton, NJ). 2010; 649:247–56.
24. Blum R, Pfeiffer F, Feick P, Nastainczyk W, Kohler B, Schafer KH, et al. Intracellular localization and in vivo trafficking of p24A and p23. Journal of cell science. 1999; 112 (Pt 4):537–48.

25. Salomonis N, Schlieve CR, Pereira L, Wahlquist C, Colas A, Zambon AC, et al. Alternative splicing regulates mouse embryonic stem cell pluripotency and differentiation. Proc Natl Acad Sci U S A. 2010; 107 (23):10514–9. https://doi.org/10.1073/pnas.0912260107 PMID: 20498046

26. Burns MB, Lackey L, Carpenter MA, Rathore A, Land AM, Leonard B, et al. APOBEC3B is an enzymatic source of mutation in breast cancer. Nature. 2013; 494(7437):366–70. https://doi.org/10.1038/nature11881 PMID: 23389445

27. Hellman NE, Spector J, Robinson J, Zuo X, Saunier S, Antignac C, et al. Matrix metalloproteinase 13 (MMP13) and tissue inhibitor of matrix metalloproteinase 1 (TIMP1), regulated by the MAPK pathway, are both necessary for Madin-Darby canine kidney tubulogenesis. The Journal of biological chemistry. 2008; 283(7):4272–82. https://doi.org/10.1074/jbc.M708027200 PMID: 18039671

28. Eggenschwiler R, Loya K, Wu G, Sharma AD, Sgodda M, Zychlinski D, et al. Sustained knockdown of a disease-causing gene in patient-specific induced pluripotent stem cells using lentiviral vector-based gene therapy. Stem cells translational medicine. 2013; 2(9):641–54. https://doi.org/10.5966/sctm.2013-0017 PMID: 23926210

29. Kanda Y. Investigation of the freely available easy-to-use software 'EZR' for medical statistics. Bone marrow transplantation. 2013; 48(3):452–8. https://doi.org/10.1038/bmt.2012.244 PMID: 23208313

30. Li M, Yu X. The role of poly(ADP-ribosyl)ation in DNA damage response and cancer chemotherapy. Oncogene. 2015; 34(26):3349–56. https://doi.org/10.1038/onc.2014.295 PMID: 25220415

31. Blackford AN, Jackson SP. ATM, ATR, and DNA-PK: The Trinity at the Heart of the DNA Damage Response. Molecular cell. 2017; 66(6):801–17. https://doi.org/10.1016/j.molcel.2017.05.015 PMID: 28622525

32. Won J, Kim M, Kim N, Ahn JH, Lee WG, Kim SS, et al. Small molecule-based reversible reprogramming of cellular lifespan. Nature chemical biology. 2006; 2(7):369–74. https://doi.org/10.1038/nchembio800 PMID: 16767085

33. Cho YS, Kim BS, Sim CK, Kim I, Lee MS. Establishment of IL-7 Expression Reporter Human Cell Lines, and Their Feasibility for High-Throughput Screening of IL-7-Upregulating Chemicals. PLoS One. 2016; 11(9):e0161899. https://doi.org/10.1371/journal.pone.0161899 PMID: 27589392

34. Shan L, Wang D, Mao Q, Xia H. Establishment of a DGKtheta Endogenous Promoter Luciferase Reporter HepG2 Cell Line for Studying the Transcriptional Regulation of DGKtheta Gene. Applied biochemistry and biotechnology. 2019; 187(4):1344–55. https://doi.org/10.1007/s12010-018-2890-4 PMID: 30229432

35. Li Z, Zhao J, Muhammad N, Wang D, Mao Q, Xia H. Establishment of a HEK293 cell line by CRISPR/Cas9-mediated luciferase knock-in to study transcriptional regulation of the human SREBP1 gene. Biotechnology letters. 2018; 40(11–12):1495–506. https://doi.org/10.1007/s10529-018-2608-2 PMID: 30232659

36. Veach RA, Wilson MH. CRISPR/Cas9 engineering of a KIM-1 reporter human proximal tubule cell line. PLoS One. 2018; 13(9):e0204487. https://doi.org/10.1371/journal.pone.0204487 PMID: 30260998

37. Li Y, Li S, Li Y, Xia H, Mao Q. Generation of a novel HEK293 luciferase reporter cell line by CRISPR/Cas9-mediated site-specific integration in the genome to explore the transcriptional regulation of the PGRN gene. Bioengineered. 2019; 10(1):98–107. https://doi.org/10.1080/21655979.2019.1607126 PMID: 31023186

38. Shinohara M, Io K, Shindo K, Matsui M, Sakamoto T, Tada K, et al. APOBEC3B can impair genomic stability by inducing base substitutions in genomic DNA in human cells. Scientific reports. 2012; 2:806. https://doi.org/10.1038/srep00806 PMID: 23150777

39. Taylor BJ, Nik-Zainal S, Wu YL, Stebbings LA, Raine K, Campbell PJ, et al. DNA deaminases induce break-associated mutation showers with implication of APOBEC3B and 3A in breast cancer kataegis. Elife. 2013; 2:e00534. https://doi.org/10.7554/eLife.00534 PMID: 23599896

40. Akre MK, Starrett GJ, Quist JS, Temiz NA, Carpenter MA, Tutt AN, et al. Mutation Processes in 293-Based Clones Overexpressing the DNA Cytosine Deaminase APOBEC3B. PLoS One. 2016; 11(5): e0155391. https://doi.org/10.1371/journal.pone.0155391 PMID: 27163364

41. Hoopes JI, Cortez LM, Mertz TM, Malc EP, Mieczkowski PA, Roberts SA. APOBEC3A and APOBEC3B Preferentially Deaminate the Lagging Strand Template during DNA Replication. Cell Rep. 2016; 14 (6):1273–82. https://doi.org/10.1016/j.celrep.2016.01.021 PMID: 26832400

42. Zhang W, Zhang X, Tian C, Wang T, Sarkis PT, Fang Y, et al. Cytidine deaminase APOBEC3B interacts with heterogeneous nuclear ribonucleoprotein K and suppresses hepatitis B virus expression. Cellular microbiology. 2008; 10(1):112–21. https://doi.org/10.1111/j.1462-5822.2007.01020.x PMID: 17672864

43. Xiao X, Yang H, Arutiunian V, Fang Y, Besse G, Morimoto C, et al. Structural determinants of APOBEC3B non-catalytic domain for molecular assembly and catalytic regulation. Nucleic acids research. 2017; 45(12):7494–506. https://doi.org/10.1093/nar/gkx362 PMID: 28575276

44. Mishra N, Reddy KS, Timilsina U, Gaur D, Gaur R. Human APOBEC3B interacts with the heterogenous nuclear ribonucleoprotein A3 in cancer cells. Journal of cellular biochemistry. 2018; 119(8):6695–703. https://doi.org/10.1002/jcb.26855 PMID: 29693745

45. Vesela E, Chroma K, Turi Z, Mistrik M. Common Chemical Inductors of Replication Stress: Focus on Cell-Based Studies. Biomolecules. 2017; 7(1).

46. Krakoff IH, Brown NC, Reichard P. Inhibition of ribonucleoside diphosphate reductase by hydroxyurea. Cancer Res. 1968; 28(8):1559–65. PMID: 4876978

47. Cheng CH, Kuchta RD. DNA polymerase epsilon: aphidicolin inhibition and the relationship between polymerase and exonuclease activity. Biochemistry. 1993; 32(33):8568–74. https://doi.org/10.1021/bi00084a025 PMID: 8395209

48. Saintigny Y, Delacote F, Vares G, Petitot F, Lambert S, Averbeck D, et al. Characterization of homologous recombination induced by replication inhibition in mammalian cells. The EMBO journal. 2001; 20 (14):3861–70. https://doi.org/10.1093/emboj/20.14.3861 PMID: 11447127

49. Ewald B, Sampath D, Plunkett W. H2AX phosphorylation marks gemcitabine-induced stalled replication forks and their collapse upon S-phase checkpoint abrogation. Molecular cancer therapeutics. 2007; 6 (4):1239–48. https://doi.org/10.1158/1535-7163.MCT-06-0633 PMID: 17406032

50. Staker BL, Hjerrild K, Feese MD, Behnke CA, Burgin AB Jr., Stewart L. The mechanism of topoisomerase I poisoning by a camptothecin analog. Proc Natl Acad Sci U S A. 2002; 99(24):15387–92. https://doi.org/10.1073/pnas.242259599 PMID: 12426403

51. Tuduri S, Crabbe L, Conti C, Tourriere H, Holtgreve-Grez H, Jauch A, et al. Topoisomerase I suppresses genomic instability by preventing interference between replication and transcription. Nature cell biology. 2009; 11(11):1315–24. https://doi.org/10.1038/ncb1984 PMID: 19838172

52. Nitiss JL. Targeting DNA topoisomerase II in cancer chemotherapy. Nature reviews Cancer. 2009; 9 (5):338–50. https://doi.org/10.1038/nrc2607 PMID: 19377506

53. Dronkert ML, Kanaar R. Repair of DNA interstrand cross-links. Mutation research. 2001; 486(4):217–47. https://doi.org/10.1016/s0921-8777(01)00092-1 PMID: 11516927

54. Koberle B, Masters JR, Hartley JA, Wood RD. Defective repair of cisplatin-induced DNA damage caused by reduced XPA protein in testicular germ cell tumours. Current biology: CB. 1999; 9(5):273–6. https://doi.org/10.1016/s0960-9822(99)80118-3 PMID: 10074455

55. Damsma GE, Alt A, Brueckner F, Carell T, Cramer P. Mechanism of transcriptional stalling at cisplatin-damaged DNA. Nat Struct Mol Biol. 2007; 14(12):1127–33. https://doi.org/10.1038/nsmb1314 PMID: 17994106

56. Borst P, Rottenberg S, Jonkers J. How do real tumors become resistant to cisplatin? Cell cycle (Georgetown, Tex). 2008; 7(10):1353–9.

57. Sedletska Y, Fourrier L, Malinge JM. Modulation of MutS ATP-dependent functional activities by DNA containing a cisplatin compound lesion (base damage and mismatch). Journal of molecular biology. 2007; 369(1):27–40. https://doi.org/10.1016/j.jmb.2007.02.048 PMID: 17400248

58. Brown R, Clugston C, Burns P, Edlin A, Vasey P, Vojtesek B, et al. Increased accumulation of p53 protein in cisplatin-resistant ovarian cell lines. International journal of cancer. 1993; 55(4):678–84. https://doi.org/10.1002/ijc.2910550428 PMID: 8406999

59. Hayashi MT, Cesare AJ, Fitzpatrick JA, Lazzerini-Denchi E, Karlseder J. A telomere-dependent DNA damage checkpoint induced by prolonged mitotic arrest. Nat Struct Mol Biol. 2012; 19(4):387–94. https://doi.org/10.1038/nsmb.2245 PMID: 22407014

60. Li H, Chang TW, Tsai YC, Chu SF, Wu YY, Tzang BS, et al. Colcemid inhibits the rejoining of the nucleotide excision repair of UVC-induced DNA damages in Chinese hamster ovary cells. Mutation research. 2005; 588(2):118–28. https://doi.org/10.1016/j.mrgentox.2005.09.005 PMID: 16290038

61. Wakasugi M, Sasaki T, Matsumoto M, Nagaoka M, Inoue K, Inobe M, et al. Nucleotide excision repair-dependent DNA double-strand break formation and ATM signaling activation in mammalian quiescent cells. The Journal of biological chemistry. 2014; 289(41):28730–7. https://doi.org/10.1074/jbc.M114.589747 PMID: 25164823

62. Stiff T, Walker SA, Cerosaletti K, Goodarzi AA, Petermann E, Concannon P, et al. ATR-dependent phosphorylation and activation of ATM in response to UV treatment or replication fork stalling. The EMBO journal. 2006; 25(24):5775–82. https://doi.org/10.1038/sj.emboj.7601446 PMID: 17124492

63. Choi S, Toledo LI, Fernandez-Capetillo O, Bakkenist CJ. CGK733 does not inhibit ATM or ATR kinase activity in H460 human lung cancer cells. DNA repair. 2011; 10(10):1000–1; author reply 2. https://doi.org/10.1016/j.dnarep.2011.07.013 PMID: 21865098

64. Williams TM, Nyati S, Ross BD, Rehemtulla A. Molecular imaging of the ATM kinase activity. Int J Radiat Oncol Biol Phys. 2013; 86(5):969–77. https://doi.org/10.1016/j.ijrobp.2013.04.028 PMID: 23726004

65. Fallone F, Britton S, Nieto L, Salles B, Muller C. ATR controls cellular adaptation to hypoxia through positive regulation of hypoxia-inducible factor 1 (HIF-1) expression. Oncogene. 2013; 32(37):4387–96. https://doi.org/10.1038/onc.2012.462 PMID: 23085754

66. Bhattacharya S, Ray RM, Johnson LR. Role of polyamines in p53-dependent apoptosis of intestinal epithelial cells. Cellular signalling. 2009; 21(4):509–22. https://doi.org/10.1016/j.cellsig.2008.12.003 PMID: 19136059

67. Suzuki T, Tsuzuku J, Hayashi A, Shiomi Y, Iwanari H, Mochizuki Y, et al. Inhibition of DNA damage-induced apoptosis through Cdc7-mediated stabilization of Tob. The Journal of biological chemistry. 2012; 287(48):40256–65. https://doi.org/10.1074/jbc.M112.353805 PMID: 23066029

68. Sakasai R, Teraoka H, Tibbetts RS. Proteasome inhibition suppresses DNA-dependent protein kinase activation caused by camptothecin. DNA repair. 2010; 9(1):76–82. https://doi.org/10.1016/j.dnarep.2009.10.008 PMID: 19959400

69. Jacquemont C, Taniguchi T. Proteasome function is required for DNA damage response and fanconi anemia pathway activation. Cancer Res. 2007; 67(15):7395–405. https://doi.org/10.1158/0008-5472.CAN-07-1015 PMID: 17671210